Physiol. Chem. Phys. & Med. NMR (20 September 2011) *41*: 1–17

The Possible Role of Cranio-Cervical Trauma and Abnormal CSF Hydrodynamics in the Genesis of Multiple Sclerosis

(Click here to view the videos of the CSF obstructions of the MS patients)

Raymond V. Damadian and David Chu

FONAR Corporation
110 Marcus Drive, Melville, NY 11747
E-mail: rvdamadian@fonar.com

Abstract: UPRIGHT® Multi-Position™ MR scanning has uncovered a key set of new observations regarding Multiple Sclerosis (MS), which observations are likely to provide a new understanding of the origin of MS. The new findings may also lead to new forms of treatment for MS. The UPRIGHT® MRI has demonstrated pronounced anatomic pathology of the cervical spine in five of the MS patients studied and definitive cervical pathology in the other three. The pathology was the result of prior head and neck trauma. All eight MS patients entered the study on a first come first serve basis without priority, and all but one were found to have a history of serious prior cervical trauma which resulted in significant cervical pathology. The cervical pathology was visualized by UPRIGHT® MRI. Upright cerebrospinal fluid (CSF) cinematography and quantitative measurements of CSF velocity, CSF flow and CSF pressure gradients in the upright patient revealed that significant obstructions to CSF flow were present in all MS patients. The obstructions are believed to be responsible for CSF "leakages" of CSF from the ventricles into the surrounding brain parenchyma which "leakages" can be the source of the MS lesions in the brain that give rise to MS symptomatology. The CSF flow obstructions are believed to result in increases in intracranial pressure (ICP) that generate "leakages" of the CSF into the surrounding brain parenchyma. In all but one MS patient, anatomic pathologies were found to be more severe in the upright position than in the recumbent position. Similarly, CSF flow abnormalities were found to be more severe in the upright position than in the recumbent position in all but one MS patient. Images of the MS patient anatomic pathologies and CSF flow abnormalities are provided with comparison images from normal examinees in Figures 1–16.

KEY WORDS: Multiple Sclerosis, Cranio-Cervical Trauma, CSF Hydrodynamics, CSF Leaks, Intracranial Pressure, CSF Peak Velocity, CSF Pressure Gradient, CSF Flow

THE ADVENT of MRI and its unique abilities to generate the tissue contrasts needed to see detail in the body's soft tissues was an important step forward in medical imaging. A particularly important example was the ability to visualize the plaque lesions of Multiple Sclerosis (1). Traditionally the symptom-generating lesions in the brain and spinal cord of Multiple Sclerosis (MS) patients are ascribed to tissue specific autoimmune interactions. These are believed to generate the parenchymal lesions of MS. More recently the advent of phase coded MR imaging has made it possible to visualize and quantify the dynamic *flow** of the cerebrospinal fluid (CSF) within the cranial vault and spinal canal.

The present inquiry originated in the course of performing UPRIGHT® MR images on a patient (patient #1, Figure 1a) with an established diagnosis of MS. It was noted that one of the MS brain lesions conspicuously appeared to be arising directly from the CSF within the lateral ventricle (Figure 1a arrow #1). An MS lesion, appearing to arise from the ventricular CSF, brought to our attention the unexplained tendency for MS lesions to be *peri-ventricular* in their distribution (2) (Figure I, Figure II). Considered conjointly, an MS lesion appearing to arise directly from ventricular CSF (Figure 1a) and the tendency of MS lesions to be *peri-ventricular* in their distribution (Figure I, Figure II) engendered the question whether abnormal CSF hydrodynamics (e.g., elevated intracranial pressure [ICP] or abnormal flow dynamics) was playing a role in the genesis of MS lesions. To address the question, eight patients with an established diagnosis of MS and seven normal examinees were studied in the FONAR UPRIGHT® Multi-Position™ MRI.

Materials and Methods

The first eight MS patients who volunteered for the study were scanned. There was no selection among MS patients. They were all scanned in the order in which they volunteered.

MRI scans were performed on a 0.6 T UPRIGHT® scanner (FONAR Corporation, Melville, NY) with a quadrature head-neck combination coil. The patient bed can be rotated to any angle between the horizontal and vertical position in the space between the two poles of the upright magnet.

Regular clinical anatomical scans of the head and neck were acquired. Ciné phase contrast scans of CSF flow were imaged using a phase contrast RF-spoiled gradient echo sequence with TR = 19-22 ms, TE = 9-12 ms, slice thickness = 8 mm, flip angle = 20-25°, matrix = 256x128 zero filled to 256x256, and NEX = 2. Data acquisition was retrospectively gated using ECG or pulse oximeter covering the entire cardiac cycle.

Thirty-two (32) uniformly spaced time frames were obtained by linear interpolation in post-processing.

To visualize the overall CSF flow pattern, a single slice of FOV = 26 cm was imaged in the midline sagittal plane. In order to quantify the CSF *flow*, an axial slice of FOV = 16 cm at the mid C-2 level and perpendicular to the spinal canal was imaged (velocity encoding along the slice-select direction, venc = 3-11 cm/s).

Quantification of CSF *flow* was accomplished by manually drawing the Region of Interest (ROI) around the spinal canal and spinal cord in the axial mid C-2 phase contrast

* flow in the absence of italics is generic, the presence of italics specifies cc/sec

scan. Phase offset was corrected by requiring the spinal cord to have zero net phase change over the whole cardiac cycle.

MR examinations of MS patients (Figures 1–8) and normal examinees (Figures 9-15) in the study were performed in both the *upright* and *recumbent* positions using the FONAR UPRIGHT® Multi-Position™ MRI. Examinees were deemed normal if they exhibited uninterrupted dorsal and ventral CSF flow on *upright* sagittal CSF flow images (e.g., Figure 15c). MS patients #7 and #8 could not be scanned recumbent. Lower limb paralysis prevented MS patient #7. Severe vertigo and emesis in the recumbent position prevented MS patient #8. CSF cinematography (ciné) was obtained both in the sagittal and axial planes. Quantitative MR measurements of CSF *flow* (cc/sec) through the spinal canal annulus obtained from axial MR images were calculated from the phase coded CSF *flow* image data. The *flow* data were obtained from axial images taken at the mid C-2 level, unless specified otherwise. The CSF velocity (cm/sec) was measured as the average annular proton velocity for each of the 32 imaging annuli acquired throughout the cardiac cycle. The peak CSF velocity was determined as the highest proton annular velocity measurement obtained for each phase (systole and diastole) of the cardiac cycle. The pressure gradient was derived from the measured CSF velocity data using the Navier-Stokes equation, with negligible contribution from the viscous term. There were three notable findings.

Results

CSF Flow Imaging and Quantification in Multiple Sclerosis Patients

The *first,* and partially expected result stemming from the MR images of MS patient #1 (Figure 1a) and the known *peri-ventricular distribution* of MS lesions (Figure I, II), was the finding of abnormal CSF flows in all eight MS patients (Figures 1–8, Table 2A, col. 10). The abnormal CSF flows corresponded with the cranio-cervical structural abnormalities found on the patients' MR images. The *second* finding was a history of severe cervical trauma prior to the patient's MS diagnosis in six of the eight MS patients and a significant possibility of cervical trauma in a seventh patient (Table 1, MS patient #8). The *third* finding was the discovery that CSF **inflow** (cc/sec) and **inflow** velocity (cm/sec) in the *upright* position is about half (53–56%) (Table 3) of what it was in the *recumbent* position in both the MS patients and normal examinees. Alperin *et al*. have shown that the average (oscillatory) CSF volume (cc) in the upright position was less than half the oscillatory volume (cc) in the supine position, but neither a reduction of CSF **inflow** velocity (cm/sec) nor of CSF **inflow** (cc/sec) in the upright position have been previously reported (3).

The first important observation of this study of eight MS patients was that *every MS patient* exhibited *obstructions to their CSF flow* when examined by phase coded CSF cinematography (ciné) in the *upright* position (Table 2A, col. 10 & 13). *All* MS patients exhibited CSF flow abnormalities that were manifest on MR cinematography as interruptions to flow or outright flow obstructions somewhere in the cervical spinal canal, depending on the location and extent of their cervical spine pathology (Table 2A, col. 10, 11 & 13). Normal examinees did not display these flow obstructions (Table 2B, col. 10 & 11).

TABLE 1. Clinical History and Symptomatology of MS Patients

1	2	3	
Patient #	History of Cranio-Cervical Trauma	Nature of Trauma	
Patient #1 (MVA #1)	Motor vehicle accident 1978 — Rear-ended by pickup truck. Patient sustained whiplash. Wore neck brace for 2 months thereafter. Passenger seat occupant hospitalized.	Whiplash injury. Cervical collar worn 2 months after accident.	
Patient #2	(1992) While patient was standing on top of a 20-ft. extension ladder repairing his home rooftop, the extension link decoupled. Ladder extension section slid groundward with patient on board. 16-oz. hammer fell 3 ft. and landed on top of patient's head. Ladder extension section then further slid to ground. Patient fell to ground hitting back of head. Patient semi-conscious and dizzy after ground impact.	Hammer hit to top of patient's head. Ladder fell backward when extension link decoupled. Patient landed hitting back of head. Semi-conscious and dizzy following impact.	
Patient #3 (MVA #2)	Major car accident 30 years ago. Rear ended by pickup truck. Car trunk collapsed to level of rear car window. Patient believes head whiplashed during accident. 2 years later second car accident, hit tree. Thrown forward on impact.	Neck and head trauma from rear-ending by pickup truck. Patient described accident as "whiplash".	
Patient #4	17 years old today – Patient age 6 years old was picked up by angry parent and shaken back and forth by shoulders. Head was caused to shake back and forth and against a wall. 8 years later (2007 age 14), hit in face by teenager which caused his right arm to go limp. Taken to Schneider's Children's Hospital, Great Neck L.I. (NSUH). Diagnosed as MS from MRI images.	Severe parental shaking age 6 (11 years prior to MS diagnosis). Exacerbating incident immediately prior to MS diagnosis (2007). Patient hit in face by teenager. Right eye bruised and right arm went limp. MRI taken immediately following injury showed multiple peri-ventricular MS lesions.	
Patient #5	No accident trauma. Ballroom ballerina/tap/ modern dance since age 3. 4–5 hours dancing/day from ages 12 to 17.	Possible dance head neck trauma. Intense dancing 1990 to 1995. MS symptoms started in 2004.	
Patient #6 (MVA #3)	Motor vehicle accident 1998 at age 19. 11 years prior to MS hit a post while driving in parking lot. Head went forward then back (reverse whiplash). Could not move neck after accident. Fractured left clavicle. Wore neck collar more than 2 weeks. Unable to move left arm. Second accident playing baseball. Hit back of neck. Blurred vision (optic neuritis) followed plus numbness in left shoulder and tingling.	Modified whiplash — head forward then back. Neck injury 11 years prior and 6 months prior. Second incident provoked symptoms.	
Patient #7 (MVA #4)	Severe car accident 1995. "Black ice". Car spun, hit divider, wrapped around tree. 2 months after accident developed spasms in each leg and impaired locomotion. Neck surgery 2003. Deteriorated markedly following surgery. Lost control of both legs. Currently wheelchair bound.	Seat belt came across left side of neck. Bruises to left neck.	
Patient #8 (MVA #5)	Age 2-3 involved in a severe motor vehicle accident that totalled the car. Patient believes she was in the customary sitting position (no seat belt or infant seat).	Possible neck injury from motor vehicle accident.	
Avg. # years trauma preceded MS diagnosis			

4	5	6
Years Physical Trauma Preceded Diagnosis	Description of MS Image Pathology	Current Symptoms
8	Two peri-ventricular MS lesions penetrating corpus callosum from lateral ventricle into adjacent brain parenchyma. Lateral ventricle swollen mid-line (Sag T2).	Loss of vision left eye — optic atrophy left eye. Loss of muscle strength both legs. Wheelchair bound.
2	Occipital horn hydrocephalus plus peri-ventricular edema i.e. "interstitial edema", MS lesions predominantly adjacent to enlarged occipital horns on both right and left.	Memory problems, sleep apnea, bladder and bowel incontinence, impotence, visual difficulties, fatigue.
21	Solitary MS lesion adjacent to left occipital horn and peri-ventricular interstitial edema anterior horns.	Transient episodes of kaleidoscopic vision, numbness left hand, frequent falling. Wears leg brace to diminish falling. Severe foot drop right foot. Severe right hand weakness. Loss of bladder control. Loss of fine motor control.
8	Multiple peri-ventricular MS lesions radiating off lateral ventricle. Multiple peri-ventricular lesions. Also pronounced interstitual edema lesions both anterior and occipital horns.	Backaches, headaches, numbness in the face. Lack of energy for 17 year old. Sleeps a lot. Gets many canker sores in mouth.
9	One lesion posterior to left occipital horn. Interstitial edema around entire ventricle. Peri-ventricular lesions.	Right arm numbness, sternal numbness. Numbness from mid-sternum to right shoulder extending to right fingertips.
11	Solitary lesion Flair Axial midway up left lateral border left ventricle, peri-ventricular interstitial edema. Possible second MS lesion adjacent occipital horn.	Tingling numbness left shoulder. Blurred vision left eye. Visual blurring after exercise.
1	Parenchymal MS appearing lesion superior to right occipital horn. Couple small peri-ventricular lesions. MS lesions adjacent to left lateral ventricle midway in AP direction. Peri-ventricular interstitial edema.	Loss of motor control lower legs. Wheelchair bound. Fatigue.
27	Multiple peri-ventricular lesions, pronounced hydrocephalus of the occipital horns of the lateral ventricles with accompanying peri-ventricular lesions and edema, prominent peri-ventricular interstitial edema and hydrocephalus in the main body of the lateral ventricles anteriorly.	Optic neuritis, severe vertigo, nausea and vomiting when supine, stumbling when walking.
11		

TABLE 2A. Anatomic Images, CSF Flow Images and CSF Flow Quantification of MS Patients

1	2	3	4	5	6	7	8	9
Patient #	Up. Peak Sys. CSF Vel. (outflow) cm/sec	Rec. Peak Sys. CSF Vel. (outflow) cm/sec	Up. Peak Dias. CSF Vel. (inflow) cm/sec	Rec. Peak Dias. CSF Vel. (inflow) cm/sec	Up. Press. Grad. Peak Peak to mmHg/cm	Rec. Press. Grad. Peak to Peak mmHg/cm	Upright MRI Image Analysis ◄---------- see glossary	Recumbent MRI Image Analysis ----------►
Patient #1 (MVA #1)	.67	**1.52** P<.05	.40	.745	.012	.024	1)C2 c.clock rot. 16°, 2)C6/7 cd.c., c.sten.	1)C2 c.clock rot. 5.7° 2)no c.sten., no cd.c.
Patient #2	**2.58** P<.05	**1.39** P<.05	**1.047** P<.05	1.033	**.054** P<.05	**.031** P<.05	1)r.lis. C5, 2)cd.c., c.sten. C5/6 3)ligfl. cd.c. C6/7, ligfl. can. obst. C6/7 4)c.sten. C6/7	1)vent. can.obs., 2)r.lis., c.sten. red. 3)ligfl. obst. absent
Patient #3 (MVA #2)	1.14	**.336**	.394	.702	.016	.011	1)r.lis. C4, C5, 2)cd.c., c.sten. C4/5,	1)r.lis. red., 2)no sp.cd. abut. C5/6
Patient #4	**1.80** P<.05	**2.71** P<.05	.464	**1.36** P<.05	**.036** P<.05	**.063** P<.05	1)sp.cd. post. 2)C3/4 dors. can.obs., 3)CTE 2mm 4)sp.cd. abut. post. wall sp.can. C3/4	1)sp.cd. more ant., 2)dors. can. pat., 3)CTE 1mm
Patient #5	**2.03** P<.05	**2.14** P<.05	**.731** P<.05	**1.55** P<.05	**.050** P<.05	**.046** P<.05	1)dsc. hrn. at C3/4, C4/5, C5/6 2)dsc. bulges at C2/3, C6/7	1)C2/3, C5/6 dsc. hrn. 2)C3/4 hrn. absent 3)C4/5less dsc. bulge 4)C6/7 dsc. bulge not present
Patient #6 (MVA #3)	.79	.94	.32	.80	.014	.020	1)CTE 2mm	1)CTE 2mm
Patient #7 (MVA #4).	.865	**—**	.51	**—**	.024	**—**	1)cd.c. C2/3 to C5/6 2)r.lis C5	1)cd.c. red. C2 to C6 2)C5 r.lis. red. (2003 conventional recumbent MRI)
Patient #8 (MVA #5)	.818	—	.380	—	.020	—	1)post. disp. sp.cd. at C2/3, obst. dors. CSFfl. at C2/3 2)markedly enlarged occipital horns lat. ventcls. 3)peri-ventcl. ed. occipital horns 4)CTE – T2 axials 5)rot. C3 c. wise	
Mean Value (MS patients)	1.34 (8 pat.)	1.51 (6 pat.)	.531 (8 pat.)	1.03 (6 pat.)	.028 (8 pat.)	.033 (6 pat.)		

a-ant., anterior; abut., abutment; **b**-bel., below; **c**-c.clock, counter clockwise; c.sten., spinal canal stenosis; c.wise, clockwise; can., canal; can.obs., spinal dors., dorsal; dsc., disc; **e**-ed., edema; **g**-grad., gradient; **h**-hrn., herniation; **i**-inter., interruption; inta., intact; **l**-lat., lateral; ligfl., ligamentum flavum; red., reduced; rot., rotation; **s**-sp., spinal; sp.cd., spinal cord; sys., systolic; **u**-unobst., unobstructed; Up., upright; **v**-vel., velocity; vent., ventral; —— **BOLDED numbers Col. 2-7** (P< .05)

10	11	12	13	
UPRIGHT MRI Ciné CSF Flow Analysis	Recumbent MRI Ciné CSF Flow Analysis	MRI Image Differences Up./Rec.	CSF Ciné Differences Up./Rec.	
←---------- see glossary ----------→				
1)dors. CSFfl. obst. at C2/3 2)vent. CSFfl. obst. C3 to C5/6, 3)vent. CSFfl. not obst. by C6/7 dsc. hrn. when Up.	1)dors. CSFfl. faint but inta., 2)vent. CSFfl. inta. to C6/7, 3)vent. CSFfl. obst. at C6/7 by disc. hrn.	1)C2 rotated 16° Up., 5.7° Rec.	1)vent. CSFfl. obst. Up. but not Rec.	1
1)dors. CSFfl. obst. top C2 to C3/4, 2)dors. CSFfl. obst. C5/6, 3)vent. CSFfl. obst. bel. C3/4	1)vent. CSFfl. obst. C3/4 & bel.	1)no infolding ligfl. Rec., 2)less c.sten. Rec.	1)CSFfl. obst. Up., 2)full circumspinal CSFfl. Rec.	2
1)dors. CSFfl. obst. C2/3 to C5/6, 2)vent. CSFfl. obst. C2/3 & bel.	1)vent. & dors. CSFfl. inta.	1)C4, C5 listhesis, much less Rec.	1)CSFfl. obst. Up., 2)CSFfl. unobst. Rec.	3
1)dors. CSFfl. obst. bel. C2/3, 2)vent. CSFfl. inta.	1)dors. CSFfl. obst. bel. C2/3, 2)vent. CSFfl. inta.	1)cord more ant. Rec.	1)same CSFfl. obst. Up. & Rec.	4
1)dors. CSFfl. obst. C2/3 to C5, 2)vent. CSFfl. obst. at C2/3, C3/4, C4/5, C5/6	1)vent. CSFfl. int. less when patient Rec.	1)C5/6 hrn. less Rec.	1)vent. CSFfl. less inter. Rec.	5
1)vent. CSFfl. obst. C2/3 to C6	1)no CSFfl. int. when patient Rec.	1)no difference	1)vent. CSFfl. obst. C2/3 to C6 Up. 2)no CSFfl. inter. Rec.	6
1)dors. CSFfl. obst. C2/3 to C4/5, 2)vent. CSFfl. obst. at C5	1)dors. CSFfl. obst. C2/3 & bel. (2003 conventional recumbent MRI)	1)less cd.c. C2 to C6, 2)r.lis. red. Rec.	1)CSFfl. obst. at C2/3 but restored at C4/5 Up. 2)not restored bel. C4/5 Rec. (2003 conventional recumbent)	7
1)dors. CSFfl. obst. C2/3				8

canal obstruction; cd.c., cord compression; cent., central; CSFfl., CSF flow; CTE, cerebellar tonsil ectopia; **d**-dias., diastolic; disp., displaced; **m**-MVA, motor vehicle accident; **o**-obst., obstructed, obstruction; **p**-pat., patent; post., posterior; press., pressure; **r**-r.lis., retrolisthesis; Rec., recumbent; ventcls., ventricles

TABLE 2B. Anatomic Images, CSF Flow Images and CSF Flow Quantification of Normal Examinees

1	2	3	4	5	6	7	8	9	
Patient #	Up. Peak Sys. CSF Vel. (outflow) cm/sec	Rec. Peak Sys. CSF Vel. (outflow) cm/sec	Up. Peak Dias. CSF Vel. (inflow) cm/sec	Rec. Peak Dias. CSF Vel. (inflow) cm/sec	Up. Press. Grad. Peak Peak to mmHg/cm	Rec. Press. Grad. Peak to Peak mmHg/cm	Upright MRI Image Analysis ←---------- see	Recumbent MRI Image Analysis glossary----------→	
Normal #1	1.07	.751	.414	.457	.021	.017			
Normal #2	.613	1.03	.332	.825	.0114	.023			
Normal #3	.752	1.05	.321	.746	.0181	.023			
Normal #4	.640	.976	.301	.626	.0135	.0135			
Normal #5	1.27	.595	.526	.488	.0227	.0126			
Normal #6	.586	.849	.325	.786	.018	.016			
Normal #7	1.32	1.022	.583	1.08	.020	.019			
Mean Value (normal examinees) (n = 7)	.893	.896	.4004	.715	.0177	.018			
+/-	.319	.172	.1124	.215	.0040	.004			

a-ant., anterior; abut., abutment; **b**-bel., below; **c**-c.clock, counter clockwise; c.sten., spinal canal stenosis; c.wise, clockwise; can., canal; can.obs., spinal dors., dorsal; dsc., disc; **e**-ed., edema; **g**-grad., gradient; **h**-hrn., herniation; **i**-inter., interruption; inta., intact; **l**-lat., lateral; ligfl., ligamentum flavum; red., reduced; rot., rotation; **s**-sp., spinal; sp.cd., spinal cord; sys., systolic; **u**-unobst., unobstructed; Up., upright; **v**-vel., velocity; vent., ventral;

10	11	12	13	
UPRIGHT MRI Ciné CSF Flow Analysis	Recumbent MRI Ciné CSF Flow Analysis	MRI Image Differences Up./Rec.	CSF Ciné Differences Up./Rec.	
←----------	see glossary	----------	----------→	
CSFfl. inta. vent. & dors.	CSFfl. inta. vent. & dors.			
CSFfl. inta. vent. & dors.	CSFfl. inta. vent. & dors.			
CSFfl. inta. vent. & dors.	CSFfl. inta. vent. & dors.			
CSFfl. inta. vent. & dors.	CSFfl. inta. vent. & dors.			
CSFfl. inta. vent. & dors.	CSFfl. inta. vent. & dors.			
CSFfl. inta. vent. & dors.	CSFfl. inta. vent. & dors.			
CSFfl. inta. vent. & dors.	CSFfl. inta. vent. & dors.			

canal obstruction; cd.c., cord compression; cent., central; CSFfl., CSF flow; CTE, cerebellar tonsil ectopia; **d**-dias., diastolic; disp., displaced; **m**-MVA, motor vehicle accident; **o**-obst., obstructed, obstruction; **p**-pat., patent; post., posterior; press., pressure; **r**-r.lis., retrolisthesis; Rec., recumbent; ventcls., ventricles

Significant differences in MS patient CSF flow cinematography (ciné) in the sagittal midplane were observed between the *upright* and *recumbent* positions, while no positional differences in ciné flow were observed in normal examinees (Table 2B, col. 10, 11 & 13). CSF flow differences between the two positions were found in the six MS patients that were scanned both upright and recumbent (Table 2A, col. 10, 11 & 13). Obstructions of spinal CSF flow in *both* the dorsal and ventral spinal canals, when viewed sagittally, were found by cinematography in five of the eight MS patients when they were examined in the *upright* position (Table 2A, patients #1, #2, #3, #5 and #7, col. 10). Patient #3 exhibited *both* dorsal and ventral CSF flow obstruction *only* in the *upright* position (Table 2A, col. 10). Dorsal and ventral CSF flows in patient #3 were unobstructed in the *recumbent* position (Table 2A, col. 11).

Regarding the quantitation of CSF *flow* (cc/sec) abnormalities, determinations of peak CSF *velocities* (cm/sec) produced the most pronounced differences between the MS patients and normal examinees (Table 2A, col. 2, 3, 4, & 5). While the peak velocity measurements in our study were measured differently than the peak velocities by Haughton *et al.* [Haughton *et al.* (4) determined the peak velocity to be the highest voxel velocity measured in the scan as compared to the highest annular velocity measured in the scan in our determination], both peak velocity methods found the peak velocity determination to be the most sensitive measure for detecting CSF *flow* abnormalities.

Among the MS patients, three of the eight patients had significantly ($P < .05$) elevated peak CSF **outflow** (systolic) *velocities* (cm/sec) from the brain (2.58, 1.80, 2.03 cm/sec) in the *upright* position (Table 2A, col. 2, patients #2, #4 and #5) compared to the mean value for the normal examinees in the *upright* position (.893 ± .32 cm/sec, Table 2B, col. 2). **Outflow** velocities for all three of these MS patients were more than twice the upright **outflow** peak velocities for the normal examinees. Four (patients #1, #2, #4, and #5) had significantly elevated peak CSF **outflow** *velocities* (cm/sec) (1.52, 1.39, 2.71 and 2.14 cm/sec, Table 2A, col. 3) in the *recumbent* position, two of which (2.71 and 2.14 cm/sec) were more than twice the normal value (.896 ± .17 cm/sec, Table 2B, col. 3). A fifth MS patient (patient #3) had a *recumbent* CSF **outflow** velocity of .336 cm/sec that was significantly reduced relative to normal (.896 ± .17 cm/sec).

In addition, two of the eight MS patients (Table 2A, col. 4, patients #2 and #5) exhibited significantly elevated peak **inflow** *velocities* in the *upright* position (Table 2A, col. 4, 1.047, and .731 cm/sec) relative to the peak **inflow** *velocities* of normal examinees (.400 cm/sec) in the *upright* position (Table 2B, col. 4). Importantly, therefore, five of the eight MS patients had at least one significantly abnormal peak CSF velocity measurement in three of the parameters measured (*upright* **outflow**, *recumbent* **outflow**, and *upright* **inflow**), and three of the MS patients exhibited elevated peak velocities in *both* the *upright* and *recumbent* positions (patients #2, #4, and #5, Table 2A, col. 2 & 3).

Sharply Reduced CSF Inflow Velocity in the Upright Position

Additionally it was found that peak CSF ***inflow*** (1.023 cc/sec) and peak CSF **inflow** *velocity* (0.400 cm/sec) (Table 3) were sharply reduced in normal examinees in the *upright* position when compared to ***inflow*** and **inflow** *velocity* in the *recumbent* position. Both peak ***inflow*** (cc/sec) and peak **inflow** *velocity* (cm/sec) in the *upright* position were found to be about half (53%–56% respectively), of what they were in the *recumbent* position (Table 3) in the normal examinees. Except for patient #2 and normal examinee #5, both

MS patients *and* the normal examinees exhibited reduced **inflow** *velocity* in the *upright* position (Table 2A, col. 4 & 5; Table 2B, col. 4 & 5). In the case of patient #2, the anticipated velocity reduction arising from the *upright* position was offset by the peak velocity acceleration arising from the patient's pathology (Table 2A, col. 4 & 8).

This *striking reduction* of CSF **inflow** into the brain in the *upright* position in both MS patients (Table 2A) and normals (Table 2B, Table 3) was unexpected, inasmuch as cerebral blood flow in normal subjects is unaffected by position (5). The observed reduction in CSF **inflow** in the *upright* position apparently constitutes normal physiology. The unexpected observation that CSF *flow* is significantly reduced in the *upright* position (or significantly increased in the *recumbent* position) raises interesting questions regarding the physiological significance of the increased CSF *flow* of recumbency.

The High Percentage of "Normal" Examinees That Did Not Qualify as Normal

Another unexpected finding was the high percentage of "normal" adults that did not qualify as **normal**. It was found that a large percentage of normal examinees (as high as 75%) did not qualify as normal with respect to their cervical spine anatomy, e.g., exhibiting localized disc herniations (or significant bulges) at C5/6 or elsewhere, or localized interruptions of CSF flow. Such examinees were entirely asymptomatic currently and historically, but were nonetheless unable to meet a standard for normal cervical spine anatomy. With the cervical spine being the most active segment of the spine, the finding, though unexpected, is not inconsistent with the cervical spine's high degree of biomechanical activity.

A Possible Physiologic Role of Nocturnal Sleep Enabled By Enhanced CSF *Flow* Into the Brain in Recumbency

Since one of the physiological roles attributed to the CSF is the delivery of nutrients to the brain and the removal of toxic metabolic waste, the increase in CSF *flow* facilitated by recumbency engenders the consideration that the normal nocturnal sleep process may in fact be playing an active role in facilitating the removal of metabolic waste from the brain and delivering nutrients. Recumbent sleep may be enabling increased CSF **inflow** into the brain for the physiologic purpose of delivering nutrients to the brain and cleansing

TABLE 3: Change of CSF Inflow With Position in Normal Examinees (see Tables 2A and 2B for velocities)

1 Peak INFLOW (cc/sec) UPRIGHT	2 Peak INFLOW (cc/sec) RECUMBENT	3 Peak INFLOW Velocity (cm/sec) UPRIGHT	4 Peak INFLOW Velocity (cm/sec) RECUMBENT
1.023	1.935	.400	.715
% Difference Up/Rec 53%		% Difference Up/Rec 56%	

it of toxic metabolic by-products*. Similarly, it may account, in some measure, for the benefits of recumbent sleep in the medical healing process.

Prior Histories of Significant and Severe Trauma

The most unexpected finding in this MR study of MS patients was the revelation that when carefully questioned, six of the eight Multiple Sclerosis patients had a prior history of severe trauma to the neck (Table 1, col. 2) with one patient (patient #2) having sustained *both* neck and head trauma. In addition, there is a significant likelihood that trauma had a role in the genesis of a seventh patient's MS (Table 1, patient #8, col. 2). The finding is consistent with prior reports that trauma may have a causative role in the onset of MS (6,7,8). All seven patients had distinct cervical anatomic pathology on their current MR images that corresponded with their trauma histories, thereby establishing that the historical trauma events contributed directly to their permanent pathologies of the cervical spine (Table 2A, col. 8 & 9) and that their cervical trauma histories *were not immaterial*. Four had received neck injuries in motor vehicle accidents, three of which were whiplash injuries, and the fourth a "reverse whiplash" (neck flexion preceding neck extension) injury (patient #7). A fifth, patient #8, was involved in a severe motor vehicle accident at age 2–3 that "totalled" the car in which she was riding without a seat belt or infant seat.

Noteworthy was the fact that the trauma and particularly motor vehicle trauma, notwithstanding its severity, was never correlated by either the patients or their physicians with the onset of their MS symptomatology. The symptoms of head and neck trauma, however, can be long lasting (e.g., 17 yrs.) (9). In all but two of the patients (patients #2 and #7, Table 1, col. 4) the trauma preceded the onset of MS symptoms by more than 8 years. When the mean value was calculated for all eight MS patients, the average number of years patient trauma preceded the patient's MS diagnosis, was 11 years. In addition, the abnormal CSF *flow* dynamics found in the MS patients of this study corresponded to the MR cervical pathology that was visualized (Table 2A, col. 2–9).

In the UPRIGHT® MRI examination of the eight MS patients, four of the eight exhibited severe cervical anatomic pathology (patients #1, #2, #3 and #7, Table 2A, col. 8). The remaining four patients had less severe but still serious cervical anatomic pathology (Table 2A, col. 8) and two (MS patients #2 [Figure 2] and #8 [Figure 8]) exhibited conspicuous swelling of the body of the cerebral lateral ventricles or of the occipital horns of the lateral ventricles.

Anatomic Pathology and CSF Flow Obstruction More Severe With the Patient Upright

In all but one (patient #6) of the seven MS patients that were imaged in both the upright and recumbent positions, the visualized anatomic pathology was more severe in the *upright* position than in the *recumbent* position (Table 2A, col. 8 & 9). Patient #1, for example, exhibited a 16° mal-rotation of C-2 on the patient's *upright* axial image (Figure 1e)

* The authors thank Charles Green, FONAR Corporation scientist and engineer, for his proposal that the increased CSF *flow* into the brain of recumbency might have the beneficial effect of enhancing CSF cleansing of the brain.

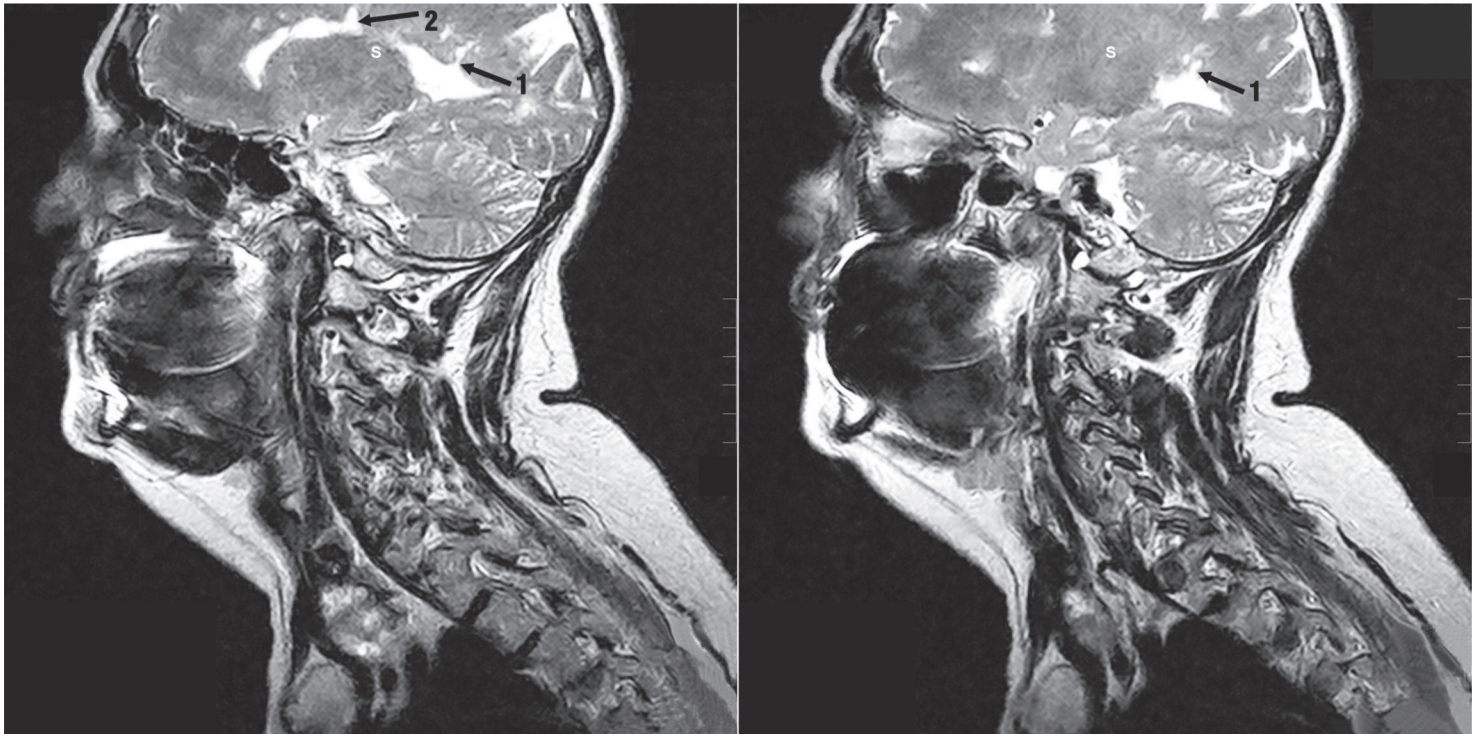

FIGURE 1a. Sagittal T2-weighted image of a Multiple Sclerosis patient (patient #1) showing two peri-ventricular MS plaques (arrows 1 & 2) perpendicular to the ventricular wall. Lesion 1 (arrow 1) exhibits an explicit connection between ventricular CSF and an MS plaque. Lesion 2 exhibits a similar connection to ventricular CSF but in a less striking manner. The images visualizing the CSF "leaks" of Figure 1a were obtained on March 11, 2010 with the patient upright in the FONAR UPRIGHT® Multi-Position™ MRI.

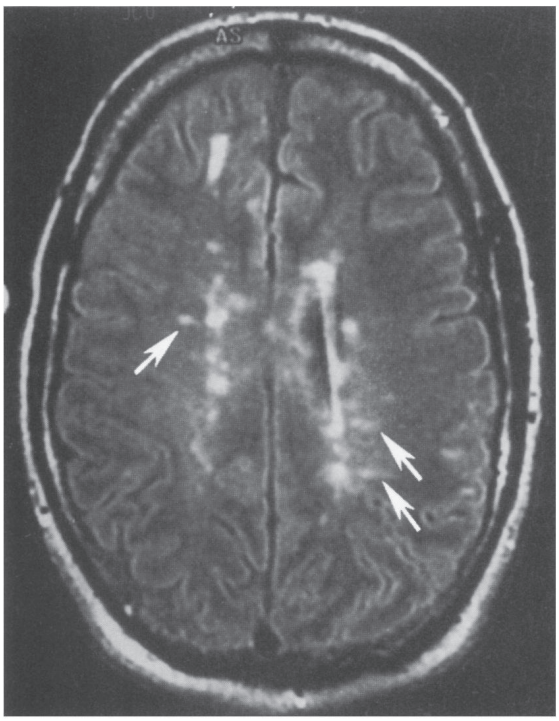

FIGURE I. (Figure 61-2, Stark, D. B., Bradley, W. B. Jr., Eds. Magnetic Resonance Imaging, Ed. III Vol. III, 1999, S. K. Lakhanpal, K. R. Maravilla, "Multiple Sclerosis", ch. 61, p. 1381, Mosby, Inc.) Axial fluid-attenuated inversion recovery (FLAIR) image at the level of the corona radiata shows multiple hyperintense MS plaques in the periventricular and subcortical white matter. Several plaques with the corona radiata demonstrate a characteristic appearance, with the long axis of the plaque oriented perpendicular to the axis of the lateral ventricles (*parallel with the white matter fibers within the corona radiata*), known as Dawson's fingers (arrows). *Noteworthy is the author's description of the plaque axis being parallel to the white matter fibers within the corona, a natural pathway for "leaking" CSF. (Author's additions to the original published legends of Figure 61-2 appear in italics.)*

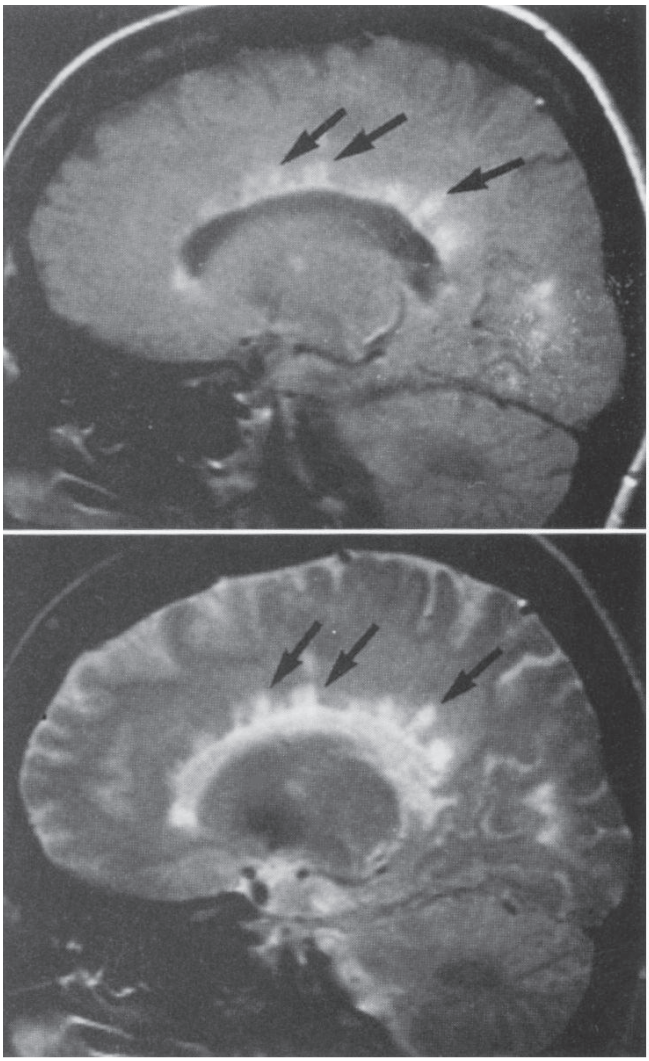

FIGURE IIA and IIB. (Figure 61-3A and 61-3B, Stark, D. B., Bradley, W. B. Jr., Eds. Magnetic Resonance Imaging, Ed. III Vol. III, 1999, S. K. Lakhanpal, K. R. Maravilla, "Multiple Sclerosis", ch. 61, p. 1381, Mosby, Inc.) Sagittal spin-density-weighted (A) and T2-weighted (B) images in a patient with MS show multiple periventricular plaques, again demonstrating the characteristic elongated appearance of the plaques oriented perpendicular to the ventricular wall (arrows). This appearance is often best demonstrated on sagittal T2-weighted images such as these. *Image B exhibits contiguity between the peri-ventricular MS plaques (arrows) and ventricular CSF. The MS plaque at the right most arrow when carefully examined exhibits a stem, similar to Figure 1a, connecting the MS plaque to ventricular CSF. (Author's additions to the original published legends of Figure 61-3A and 61-3B appear in italics.)*

CLICK ON IMAGES WITH A BLUE BORDER TO VIEW MRI CINES (MOVIES)

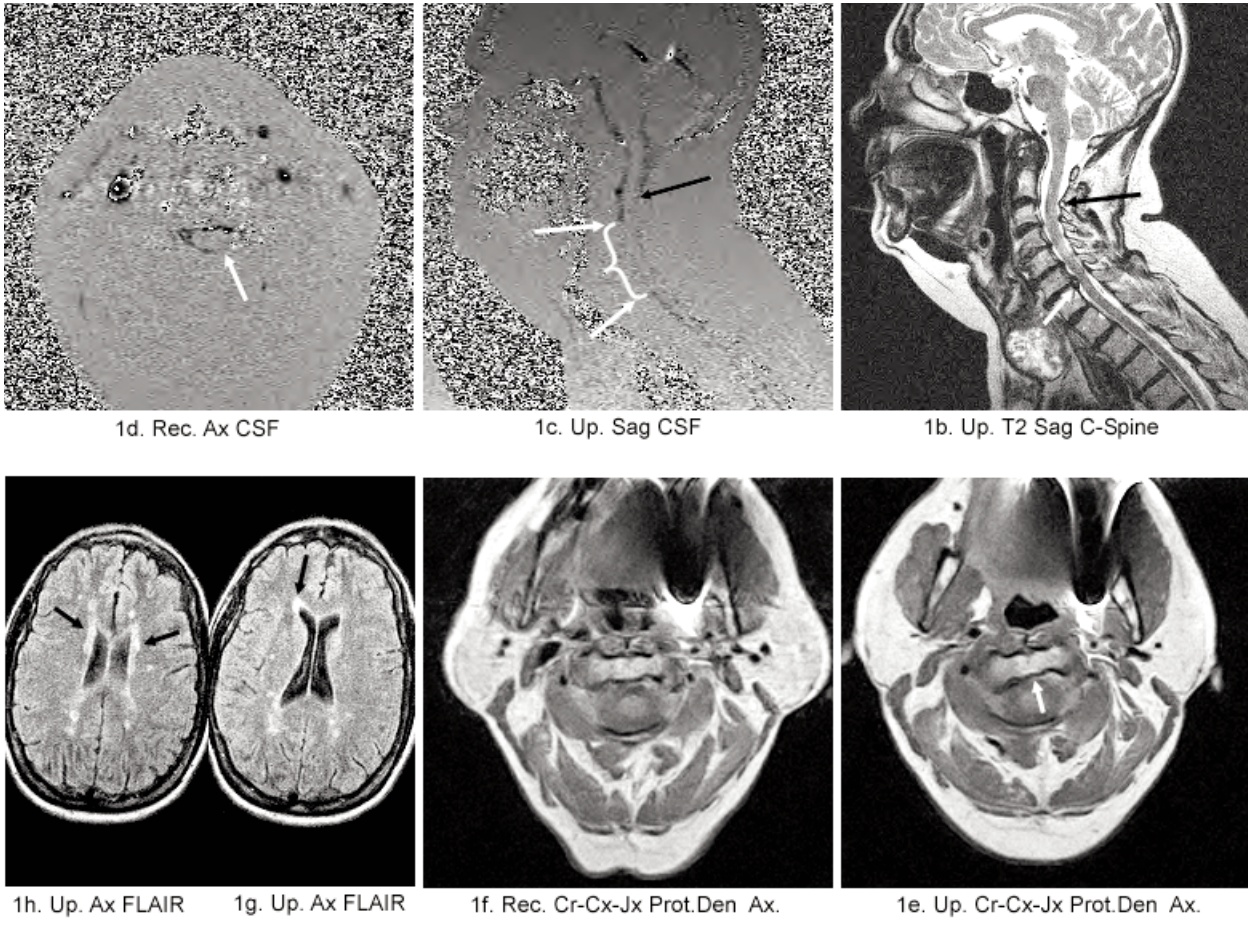

FIGURE 1b–1h. The first MS patient (patient #1) exhibited peri-ventricular MS lesions (Figures 1g & 1h) that were adjacent to the occipital horns of the lateral ventricles as well as to the anterior horns. Additionally, MS patient #1 exhibited a non-uniform distribution of peri-ventricular interstitial edema (PVIE). Peri-ventricular interstitial edema suggestive of CSF leakage was present anterolaterally in both right and left lateral ventricles in the axial image of Figure 1h (black arrows) and was most pronounced adjacent to the anterior horn of the right lateral ventricle (Figure 1g black arrow). The patient also exhibited a sixteen degree (16°) counter-clockwise rotation of C2 in the upright position (Figure 1e white arrow) which reduced to a five degree (5°) rotation in the recumbent position (Figure 1f). Additionally, disc herniations and disc protrusions were observed to be present in the upright position at all cervical levels from C2/3 to C6/7 (Figure 1b) with the most prominent protrusions/herniations occurring at C4/5, C5/6, and C6/7 abutting the spinal cord and obstructing the ventral spinal canal. The disc herniation and cord abutment at C6/7 was the most pronounced (Figure 1b white arrow). An impediment to dorsal CSF flow manifest as hypertrophy and infolding of the ligamentum flava at C2/3 and C3/4 dorsally (Figure 1b black arrow) was also visualized.

The visualized anatomic obstructions of the dorsal and ventral spinal canals resulted in corresponding dorsal and ventral interruptions of CSF flow in the spinal canal (Figure 1c). Axial CSF flow measured in the recumbent position at C4 was interrupted from 1 o'clock to 6 o'clock in the left lateral spinal canal (Figure 1d white arrow).

CLICK ON IMAGES WITH A BLUE BORDER TO VIEW MRI CINES (MOVIES)

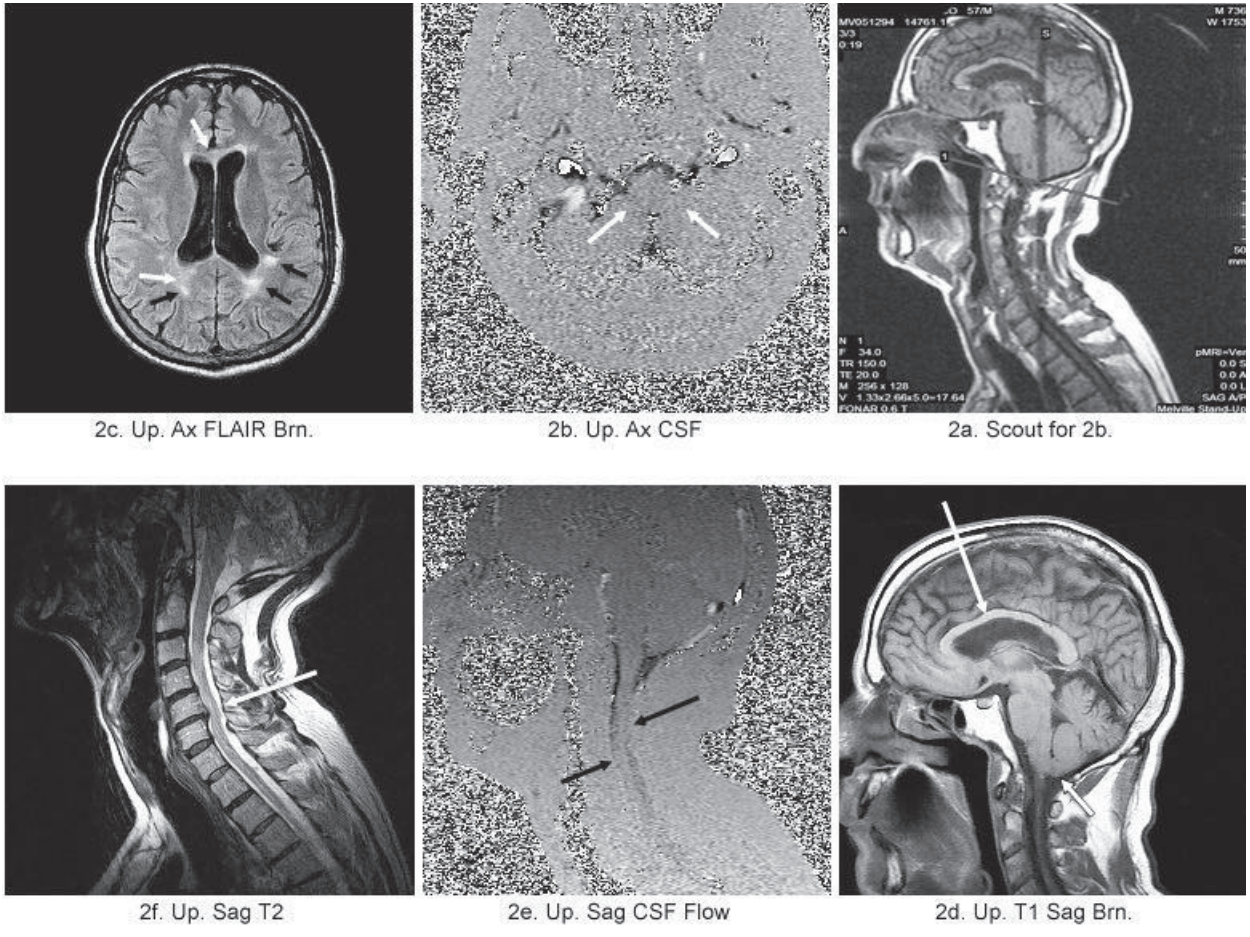

FIGURE 2a–2f. MS patient #2 exhibited MS lesions adjacent to both occipital horns of the lateral ventricles (Figure 2c black arrows), MS lesions adjacent to both anterior horns (Figure 2c) and hydrocephalus of the lateral ventricles (Figure 2c) and (Figure 2d white arrow). The presence of non-uniform peri-ventricular interstitial edema at the anterior horns was also evident (Figure 2c white arrow). Anatomically, cerebellar tonsil ectopia (CTE) was seen abutting the brainstem (Figure 2b white arrows) and was manifest as incomplete and dorsally obstructed CSF flow in the posterior foramen magnum secondary to cerebellar tonsil obstruction (Figure 2b white arrows).

Additionally, anatomic impedance and obstruction of CSF in the ventral spinal canal (Figure 2f opposite white arrow) was visualized at C5 and C4 secondary to a posterolisthesis of C5 and a disc herniation abutting and posteriorly displacing the spinal cord at C5/6. The anatomic CSF obstruction of the ventral spinal canal visualized in the patient's upright sagittal image of the cervical spine (Figure 2f opposite white arrow) was manifest as corresponding impairments of CSF flow ventrally and dorsally from C4 to C5 (Figure 2e black arrows).

CLICK ON IMAGES WITH A BLUE BORDER TO VIEW MRI CINES (MOVIES)

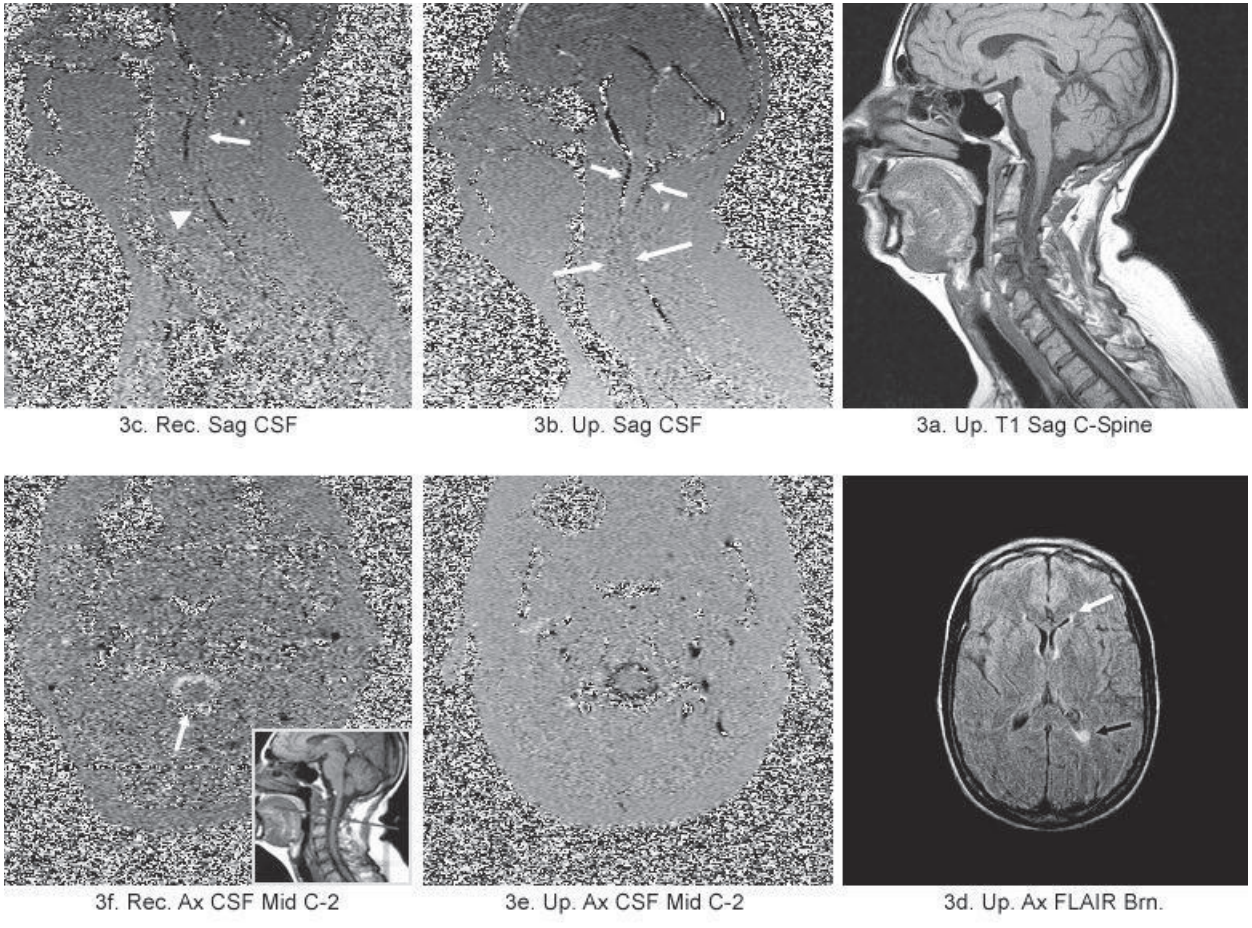

FIGURE 3a–3f. MS patient #3 exhibited an MS lesion adjacent to the occipital horn of the left lateral ventricle (Figure 3d black arrow) and enhanced peri-ventricular interstitial edema at the anterior horns (white arrow). Anatomical degradation of cervical vertebra C4 and C5 and obstructive disruption of the spinal canal at this level is visualized in the upright image of the cervical spine (Figure 3a). Dorsal and ventral CSF flow is likewise interrupted at C4 and C5 (Figure 3b long white arrows). Dorsal and ventral CSF flow is unobstructed anatomically at C2 (Figure 3a) in the upright position and unobstructed both sagittally (Figure 3b short white arrows) and axially (Figure 3e) with respect to CSF flow in the upright position. In the recumbent position, however, CSF flow is obstructed dorsally at C2 (Figure 3f white arrow), in contrast to unobstructed dorsal CSF flow at C2 when the patient is upright (Figure 3e). CSF flow in the recumbent position (Figure 3c white arrowhead), however, is also obstructed ventrally at the same C4 and C5 cervical levels that exhibit the anatomic disintegration visible in the upright MR images of the patient's cervical spine (Figure 3a).

CLICK ON IMAGES WITH A BLUE BORDER TO VIEW MRI CINES (MOVIES)

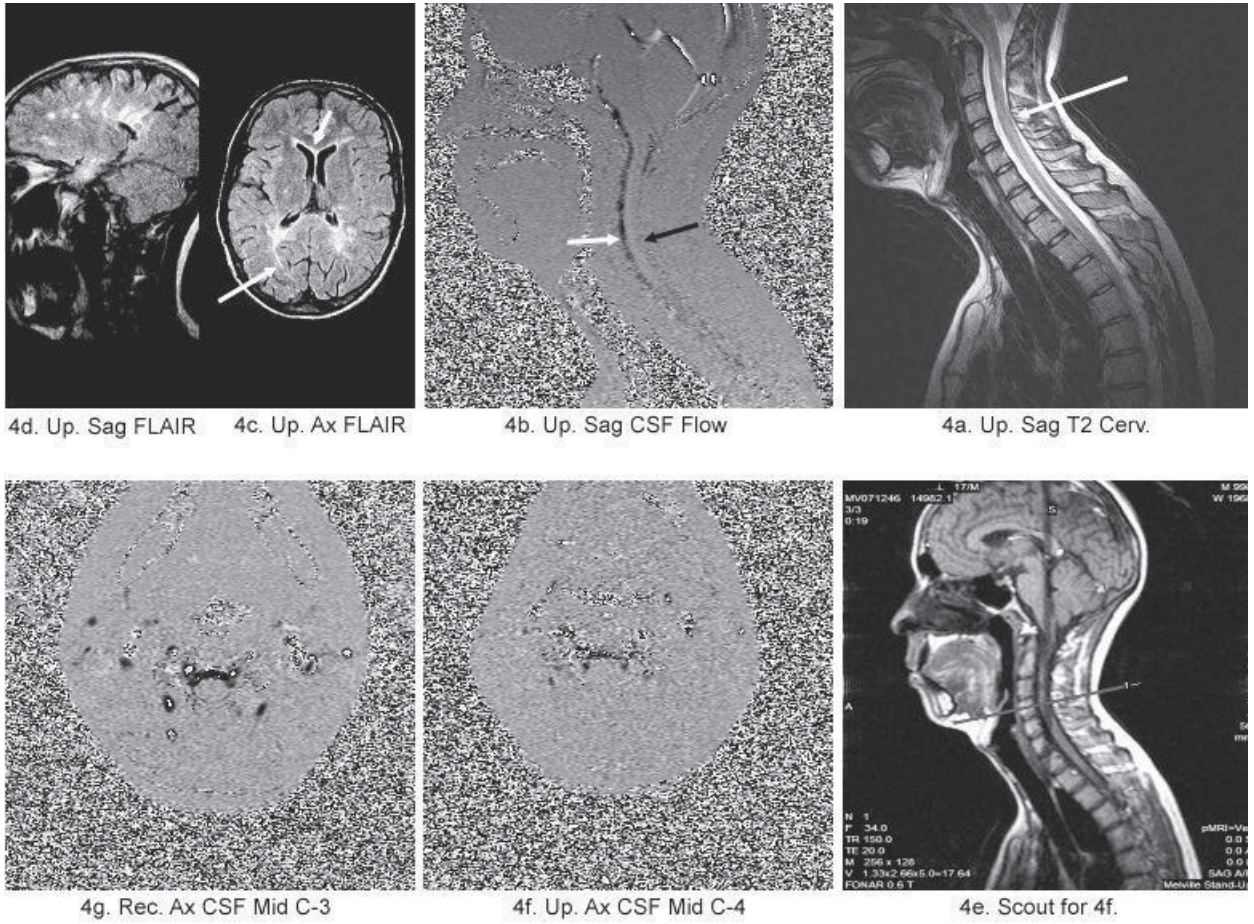

FIGURE 4a–4g. MS patient #4 exhibited a pronounced aggregate of MS lesions in peri-ventricular distribution around the lateral ventricles (Figure 4d and 4c) increasing in frequency in the direction of the occipital horns (Figure 4d black arrow). Irregular peri-ventricular interstitial edema is pronounced at the anterior horns (Figure 4c short white arrow). The density of MS lesions is most pronounced adjacent to the occipital horns (Figure 4c) where, in addition, what appears to be a CSF "leakage" striation (Figure 4c) arising from the right occipital horn (white arrow) is conspicuous and suggestive of an increase in ventricular CSF pressure within the lateral ventricle. Patient #4 also exhibits a posterior displacement of the spinal cord within the spinal canal abutting the posterior wall of the spinal canal (Figure 4a) at the level of cervical disc C3/4 (white arrow). The anatomic obstruction of the dorsal spinal canal resulting from the posterior displacement of the spinal cord and its abutment of the posterior wall of the canal (Figure 4a), is accompanied by an obstruction of dorsal CSF flow in the spinal canal (Figure 4b black arrow). Axial MR images of the spinal canal taken in both the upright position (Figure 4f) and in the recumbent position (Figure 4g) exhibit a corresponding absence of dorsal CSF flow in the upright position (Figure 4f) at the mid C-4 level (Figure 4e and 4f) and also at the mid C-3 level in the recumbent position (Figure 4g).

CLICK ON IMAGES WITH A BLUE BORDER TO VIEW MRI CINES (MOVIES)

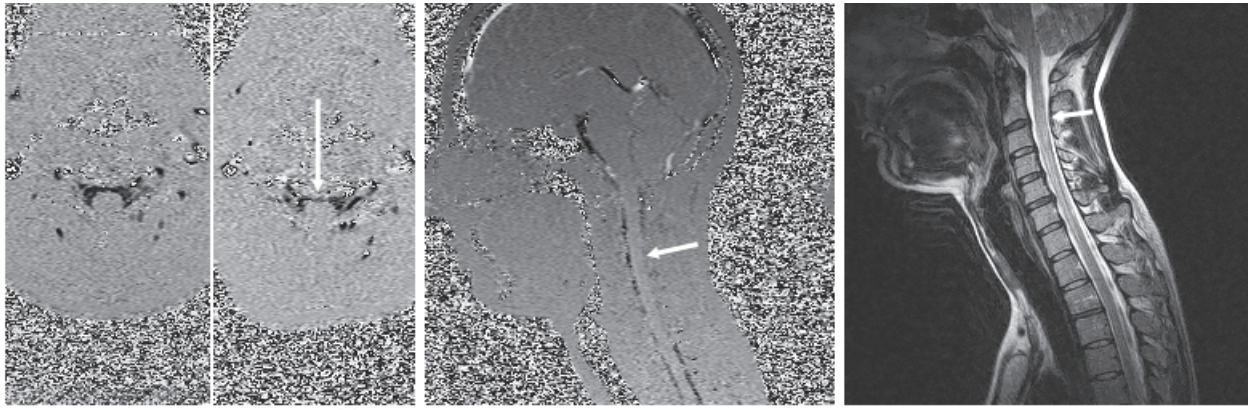

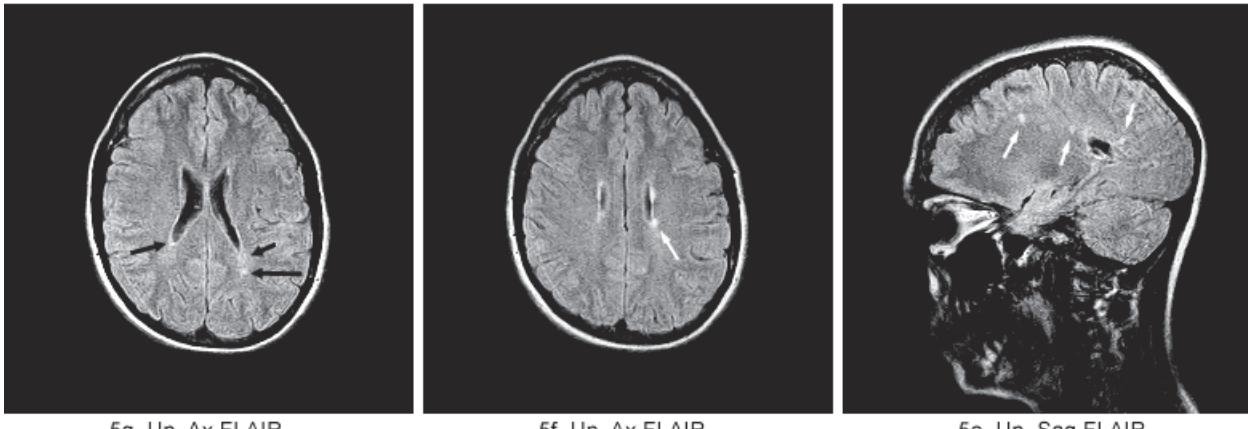

FIGURE 5a–5g. MS patient #5 exhibited peri-ventricular MS lesions (Figure 5e white arrows) on the upright sagittal FLAIR images of the brain. The upright axial FLAIR images (Figures 5g and 5f) show MS lesions adjacent to the left occipital horn of the lateral ventricle (Figure 5g black arrow) and lesions attached to the lateral wall of the left ventricle (Figure 5f white arrow). Additionally, irregular peri-ventricular interstitial edema is present most pronounced in the right occipital horn (Figure 5g black arrow), with the additional suggestion of CSF "leakage" (Figure 5g small black arrow) suggestive of an increase in intraventricular CSF pressure connecting the left occipital horn to the MS lesion. Anatomically, MS patient #5 exhibited cervical disc bulges indenting the thecal sac and anatomically interfering with CSF flow at C4/5, C5/6 and C6/7 (Figure 5a). Direct cervical disc abutment of the spinal cord is exhibited at C5/6. Correspondingly, CSF flow is interrupted ventrally at C2/3, C3/4, C4/5, C5/6 and C6/7 in the upright sagittal images of CSF flow (Figure 5b). Additionally, significant compromise of the dorsal spinal canal at C2/3 (Figure 5a white arrow) that appears obstructive of CSF is manifest as an obstruction and absence of CSF flow dorsally from C2/3 to C6/7 (Figure 5b white arrow). The axial image of CSF flow obtained at mid C-3 (Figure 5c) exhibits an absence of CSF flow dorsally but satisfactory ventral flow (Figure 5c white arrow) corresponding with the upright CSF flow imaging of the sagittal plane that exhibits disc interrupted ventral CSF flow but absent dorsal CSF flow (Figure 5b white arrow). The recumbent axial imaging of CSF flow (Figure 5d) exhibits increased annular flow compared to CSF flow in the upright position at C3 (Figure 5c) but the same annular distribution of CSF flow that shows intact ventral flow but absent dorsal flow.

CLICK ON IMAGES WITH A BLUE BORDER TO VIEW MRI CINES (MOVIES)

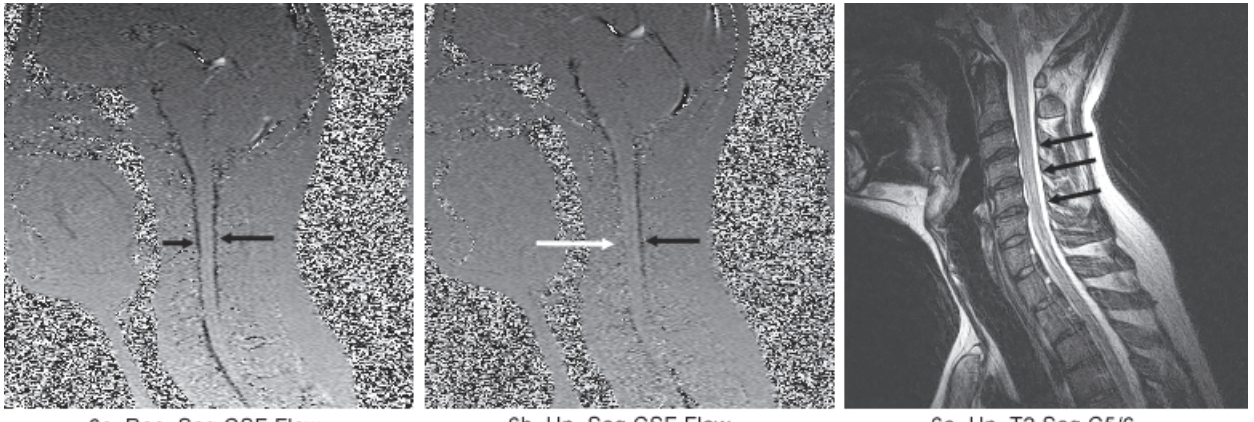

6c. Rec. Sag CSF Flow 6b. Up. Sag CSF Flow 6a. Up. T2 Sag C5/6

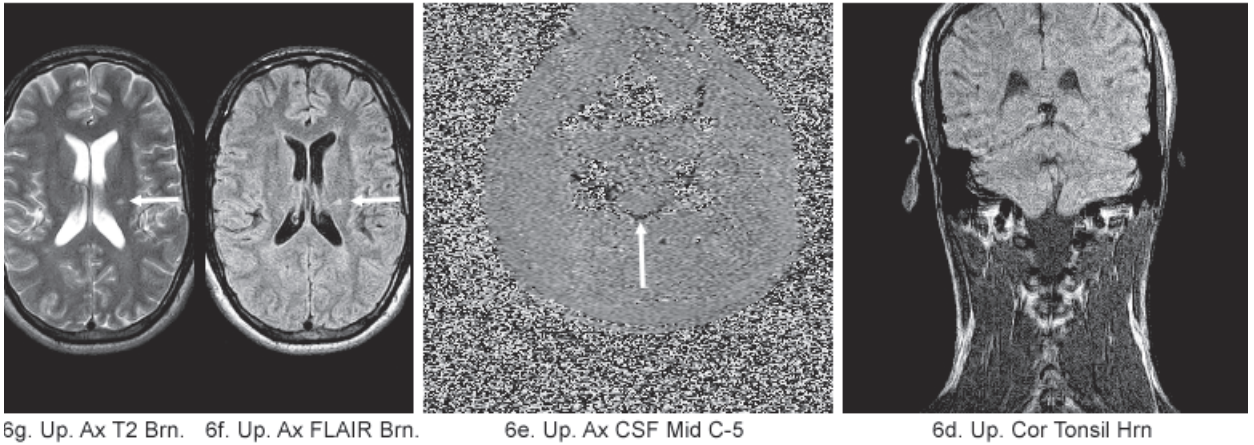

6g. Up. Ax T2 Brn. 6f. Up. Ax FLAIR Brn. 6e. Up. Ax CSF Mid C-5 6d. Up. Cor Tonsil Hrn

FIGURE 6a–6g. MS patient #6 exhibited an MS lesion proximate to the wall of the left lateral ventricle (Figure 6f & 6g white arrows). CSF flow in the dorsal spinal canal is unobstructed anatomically in the upright position (Figure 6a) and correspondingly unobstructed in the dynamic images of dorsal CSF flow (Figure 6b black arrow). Obstruction of ventral CSF flow (Figure 6b white arrow) in the upright position corresponding to the cervical disc herniations (Figure 6a) that obstruct the ventral spinal canal and abut the spinal cord is evident in Figure 6b. The cervical disc herniations at C3/4, C4/5 and C5/6 responsible for the obstruction are visualized in the upright T2 image of the cervical spine (Figure 6a black arrows) where they are seen indenting the thecal sac abutting the cord and anatomically obstructing the CSF ventrally (Figure 6a). The ventral CSF flow obstruction of MS patient #6 is visible only with the patient upright. When weight loading of the C-spine is removed with the patient in the recumbent position (Figure 6c), CSF flow is restored ventrally and both normal dorsal and ventral CSF flow are simultaneously visualized (Figure 6c black arrows).

CLICK ON IMAGES WITH A BLUE BORDER TO VIEW MRI CINES (MOVIES)

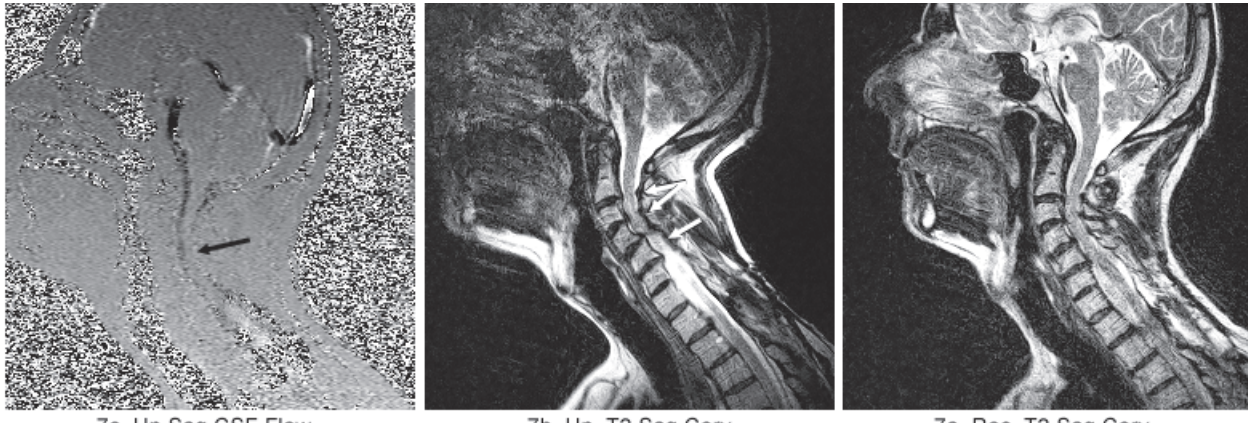

7c. Up.Sag CSF Flow | 7b. Up. T2 Sag Cerv. | 7a. Rec. T2 Sag Cerv.

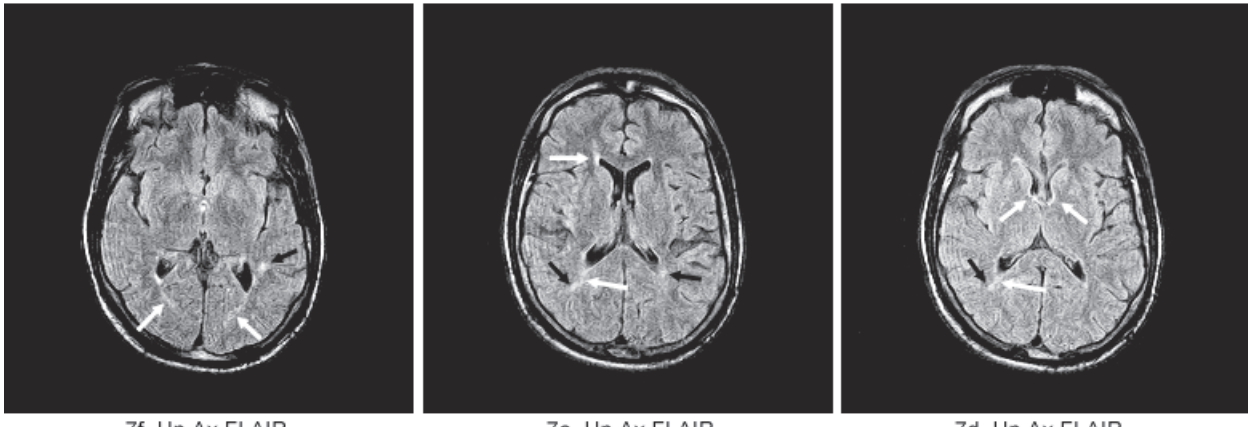

7f. Up.Ax FLAIR | 7e. Up.Ax FLAIR | 7d. Up.Ax FLAIR

FIGURE 7a–7f. MS patient #7 exhibited MS lesions adjacent to the left occipital horn (Figure 7f & 7e black arrows) and proximate to the right occipital horn (Figure 7d & 7e small black arrow). Additionally, striations suggestive of CSF "leakages" appear in the upright axial FLAIR images of patient #7 (Figure 7f, 7e and 7d white arrows). Also present is an irregular peri-ventricular interstitial edema suggestive of increased intracranial pressure that is exhibited as hyperintensities contiguous with the anterior horns of the lateral ventricle. The hyperintensity is most pronounced contiguous with the right anterior horn of the lateral ventricle (Figure 7e anterior white arrow). The peri-ventricular edema is also visible contiguous with the lateral walls of the left and right anterior horns of the lateral ventricles (Figure 7d anterior white arrows).

Anatomically severe compression of the spinal cord is visible in MS patient #7 from C2/3 to C5/6 obstructing the ventral spinal canal. The disc compressions of the cord (Figure 7a) are further compounded by an additional retrolisthesis of C5 when the patient is upright (Figure 7b) that compresses the cord further and displaces it posteriorly to a greater extent in the upright position (Figure 7b white arrow) under the added weight load. Additionally, hypertrophies of the ligamentum flavum (Figure 7b intersecting white arrows) compress the spinal cord dorsally and obstruct the dorsal canal (Figure 7a).

The dynamic upright imaging of CSF flow (Figure 7c) exhibits a corresponding obstruction of CSF flow dorsally (Figure 7c black arrow) from C2/3 to C4/5 and impairs CSF flow ventrally in the same region.

CLICK ON IMAGES WITH A BLUE BORDER TO VIEW MRI CINES (MOVIES)

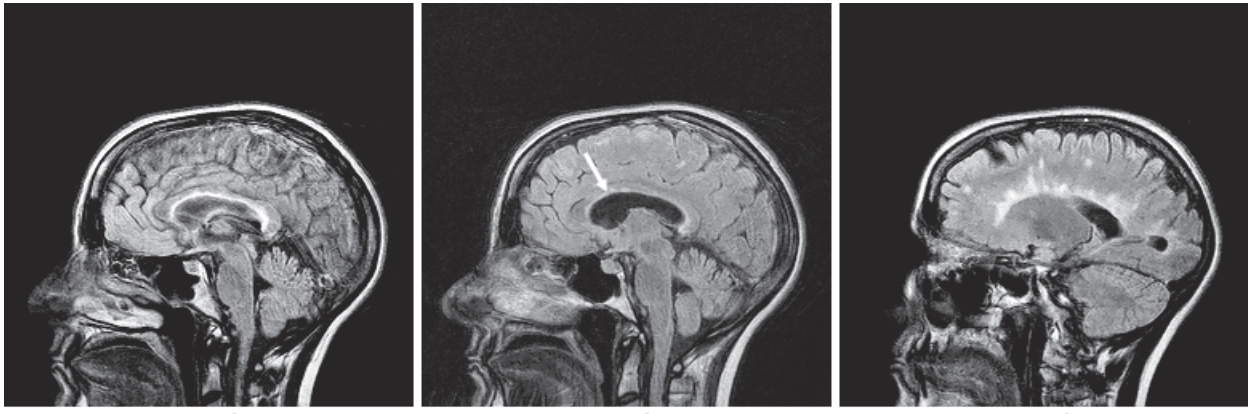

8c. Up. Flair Sag Brn. 8b. Up. Flair Sag Brn. 8a. Up. Flair Sag Brn.

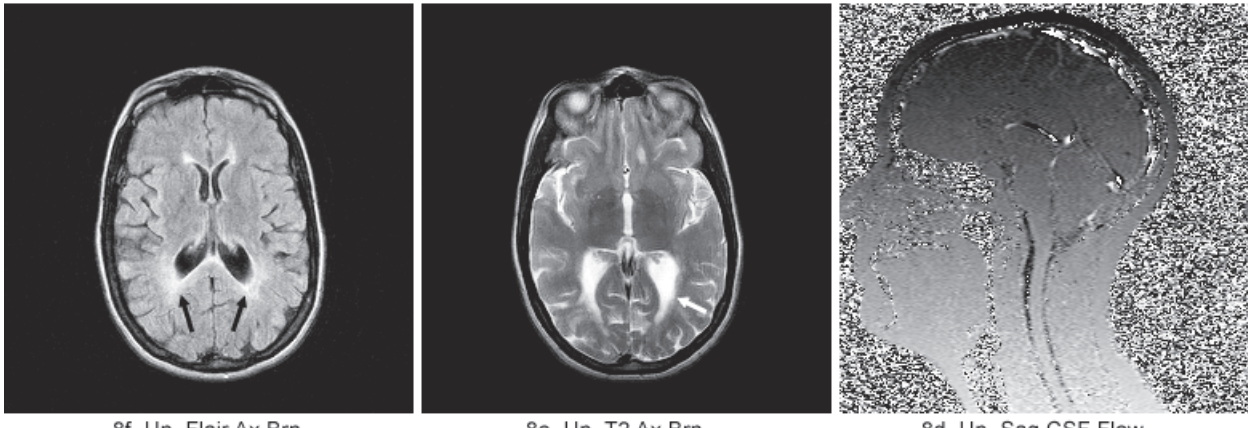

8f. Up. Flair Ax Brn. 8e. Up. T2 Ax Brn. 8d. Up. Sag CSF Flow

FIGURE 8a–8f. MS patient #8 exhibited a pronounced peri-ventricular distribution of MS lesions (Figure 8a). In addition, multiple cerebral pathologies suggestive of increased intracranial pressure (ICP) were seen. Most conspicuous was the hydrocephalus of the occipital horns of the lateral ventricles visualized in the Upright T2 axial images of the brain (Figure 8e white arrow) and in axial Flair images of the brain (Figure 8f). Particularly prominent was the pronounced edema seen adjacent to the occipital horns of the lateral ventricles (Figure 8f black arrows) strongly suggestive of CSF "leakage", possibly secondary to an increased ICP, into the surrounding brain parenchyma. Similarly, the conspicuous collar of interstitial edema surrounding the lateral ventricles in the upright Flair sagittal image of the brain (Figure 8c) and the conspicuous ventricular dilatation of the body of the lateral ventricles (Figure 8b white arrow) are further suggestive of an increased intracranial pressure (ICP) being the origin of the CSF "leakage" seen in Figures 8e and 8f.

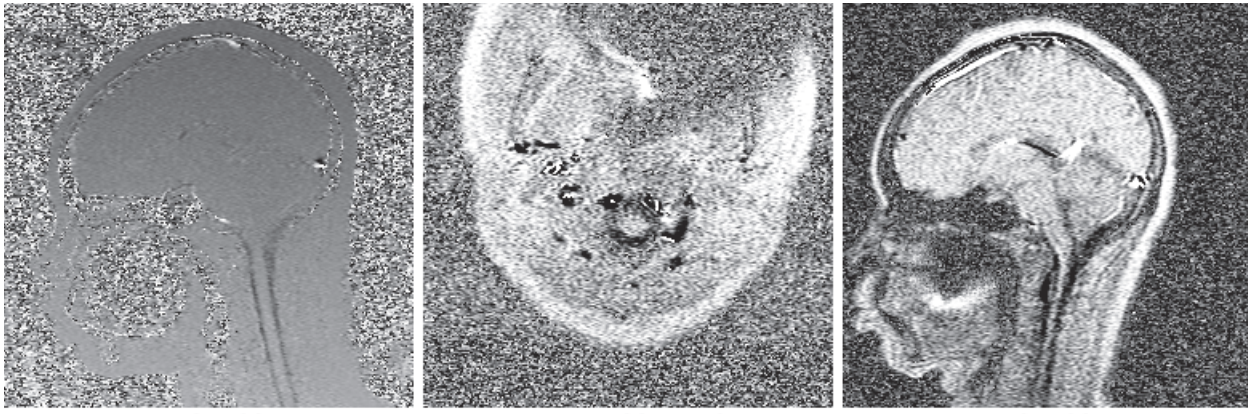

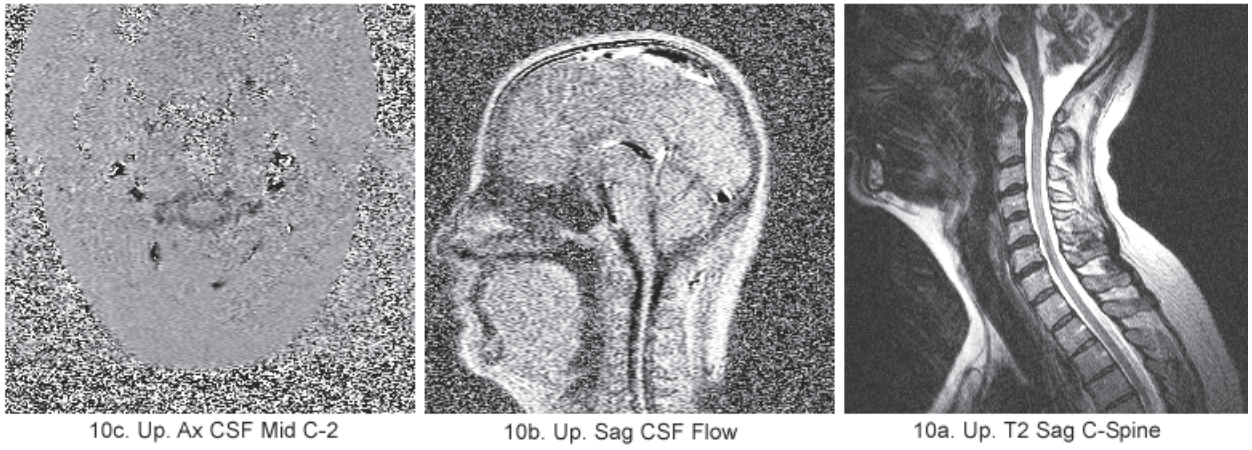

FIGURE 9a–9c. UPRIGHT® normal examinee #1 exhibits continuous ventral and dorsal sagittal CSF flow (Figure 9a & 9c black channels) as well as uninterrupted 360° annular circumspinal flow (black annulus) visualized in the axial image obtained at mid C-2 (Figure 9b).

FIGURE l0a–10c. UPRIGHT® normal examinee #2 shows full patency of the ventral and dorsal spinal canals (Figure 10a) manifest as uninterrupted ventral and dorsal sagittal CSF flow (Figure l0b black channels) and as uninterrupted 360° annular circumspinal CSF flow in the axial image obtained at mid C-2 (Figure 10c black annulus).

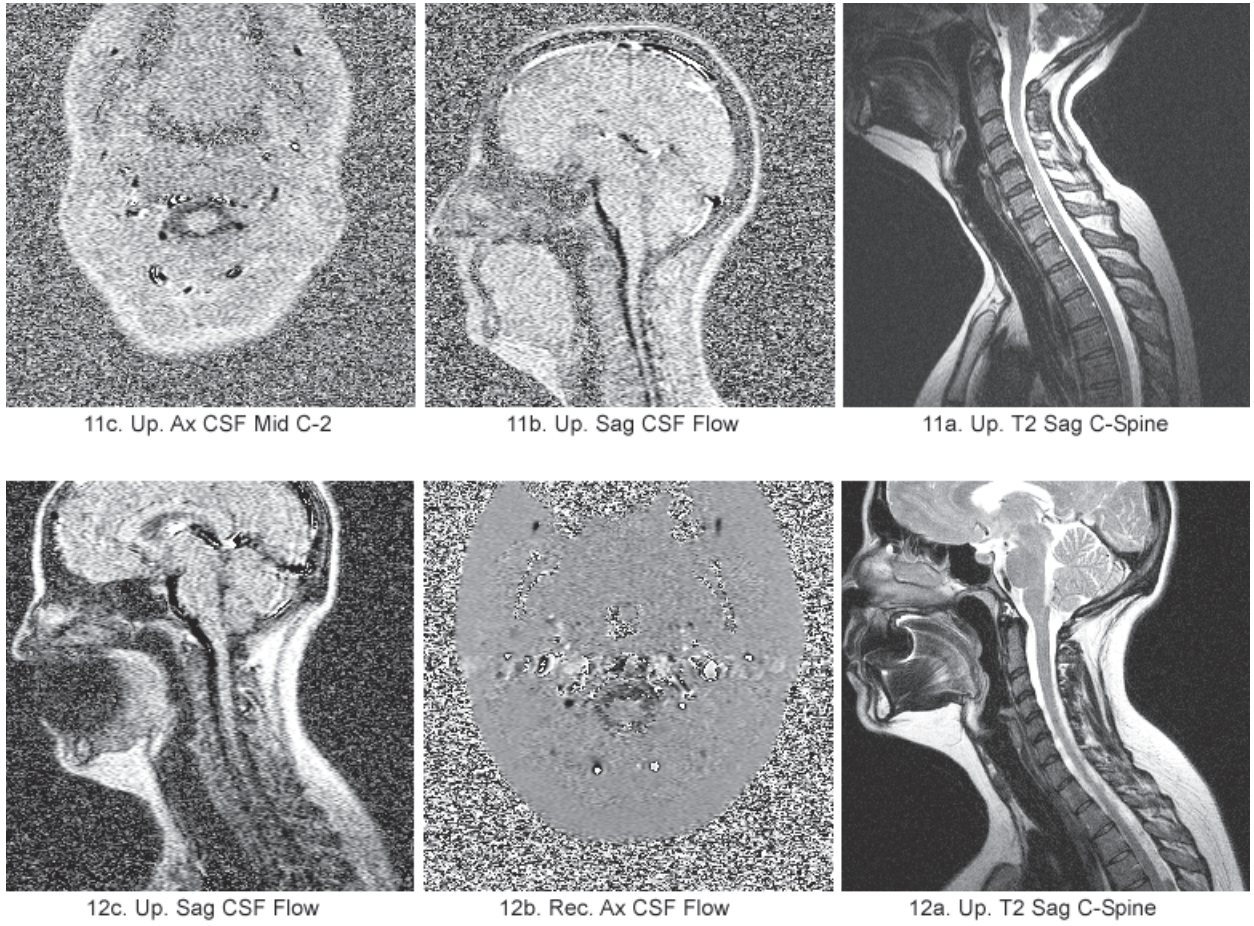

FIGURE 11a–11c. UPRIGHT® normal examinee #3 exhibits patent ventral and dorsal spinal canals (Figure 11a) confirmed by intact ventral and dorsal CSF flow in upright sagittal CSF flow (Figure 11b black channels) and full 360° annular circumspinal CSF flow in the axial image obtained at mid C-2 (Figure 11c black annulus).

FIGURE 12a–12c. UPRIGHT® normal examinee #4 exhibits patent ventral and dorsal spinal canals (Figure 12a) with full UPRIGHT® ventral and dorsal CSF flow (Figure 12c black channels) and full 360° annular circumspinal recumbent CSF flow in the axial image obtained at mid C-2 (Figure 12b black annulus).

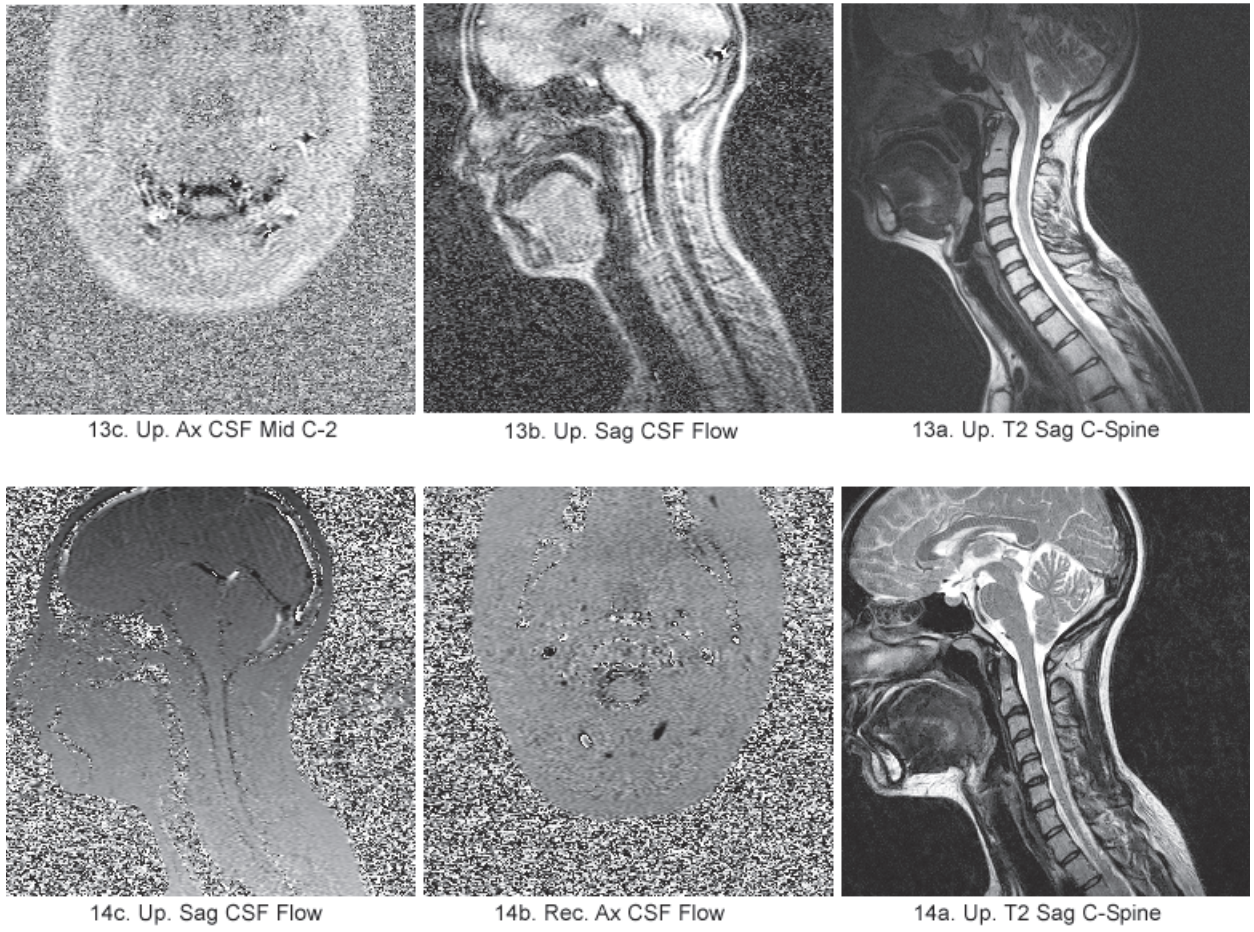

FIGURE 13a–13c. UPRIGHT® normal examinee #5 exhibits patent vemtral and dorsal spinal canals (Figure l3a) visualized as uninterrupted UPRIGHT® CSF flow ventrally and dorsally in the sagittal CSF image (Figure 13b black channels) as well as in full 360° annular circumspinal CSF flow in the UPRIGHT® axial image obtained at mid C-2 (Figure l3c black annulus).

FIGURE 14a–14c. UPRIGHT® normal examinee #6 exhibits patent ventral and dorsal spinal canals (Figure 14a) confirmed by uninterrupted ventral and dorsal CSF flow in the UPRIGHT® sagittal image of CSF flow (Figure 14c black channels) and by full 360° annular circumspinal CSF flow in the axial recumbent image obtained at mid C-2 (Figure 14b black annulus).

CLICK ON IMAGES WITH A BLUE BORDER TO VIEW MRI CINES (MOVIES)

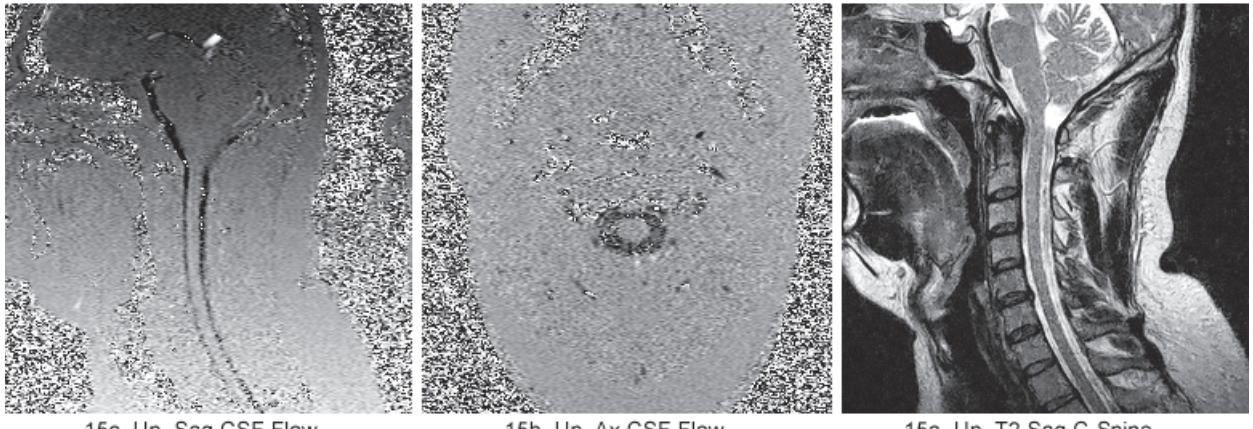

FIGURE 15a–15c. UPRIGHT® normal examinee #7 exhibits patent ventral and dorsal CSF channels (Figure 15a) confirmed by full 360° annular circumspinal CSF flow in the UPRIGHT® axial image obtained at mid C-2 (Figure 15b black annulus) and by the uninterrupted ventral and dorsal CSF flows exhibited in the UPRIGHT® sagittal CSF flow study (Figure 15c black channels).

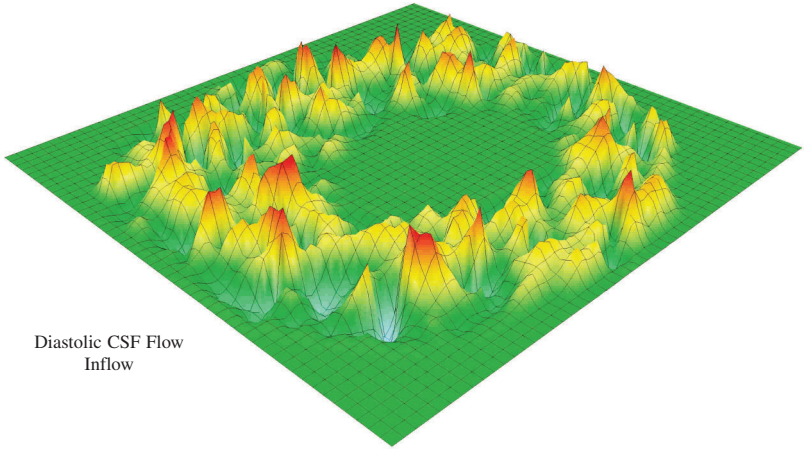

Pre-treatment
Figure 16a

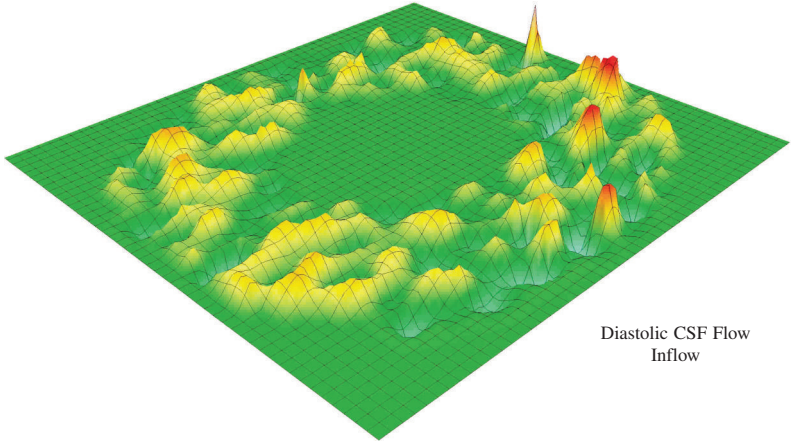

Post-treatment
Figure 16b

CSF Pixel* Velocities at mid C-2 in MS Patient #8 Before and After Successful Treatment.

The malalignment of C-1 found by the FONAR UPRIGHT® MRI images of the cervical spine of MS patient #8 in the upright position was successfully treated by Dr. Scott Rosa, using the Atlas Orthogonal (AO) instrumentation. She is the first MS patient of this study of MS patients that has been treated thus far. The patient's symptoms, severe vertigo accompanied by vomiting when recumbent and stumbling from unequal leg length, ceased upon treatment. Figure 16a are the pixel* velocity maps of CSF in the peri-spinal CSF annulus at mid C-2 in the upright symptomatic patient prior to treatment. The CSF void in the center is the spinal cord. Figure 16b are the pixel velocity maps of the upright asymptomatic patient immediately following treatment with the AO instrument. Pixel velocities were obtained from the axial CSF flow MR images obtained at C-2. Figure 16b exhibits an overall reduction in CSF velocity as well as a distinct reduction in the number of CSF flow jets (red), compared to the number of flow jets present in the symptomatic patient prior to treatment (Figure 16a). In addition, average CSF velocity (average peak height) was reduced in the asymptomatic MS patient following treatment as compared to the symptomatic patient prior to treatment. CSF Flow was also more homogeneous (less peak height variation) in the asymptomatic patient than in the symptomatic patient. The CSF pixel velocities of Figure 16 were computed and mapped by FONAR scientists-engineers Michael Boitano and Bob Wolf. The CSF flow measurements obtained immediately following successful AO treatment of the patient and the cessation of her MS symptoms also exhibited a 28.6% reduction of the patient's measured CSF pressure gradient. The patient is currently being maintained free of MS symptoms (vertigo and vomiting on recumbency) by weekly treatments with the AO instrument.

* 3D pixels (voxels)

Dolar, M.T., Haughton, V.M., Iskandar, B.J. and Quigley, M. (2004) Am. J. Neuroradiol., 25:142 reported analogous reductions in CSF pixel velocities in Chiari I patients after surgical decompression.

that reduced to a 5.7° rotation (Figure 1e & 1f) when the patient was *recumbent*. Another example is patient #2. In patient #2, the spinal canal stenosis in the *upright* position at C5/6 (Figure 2f opposite white arrows; Table 2A, col. 8), that was the result of disc herniation, osteophyte compression and retrolisthesis of C-5 obstructing the anterior spinal canal, was further compounded in the upright position by anterior infolding of the ligamentum flavum obstructing the dorsal spinal canal at C5/6 and at C6/7. The canal stenosis in patient #2 was substantially reduced in the *recumbent* position where the ligamentum flavum infolding became non-existent and non-obstructive of the dorsal spinal canal when the patient was *recumbent* (Table 2A, col. 8 & 9). See Table 2A, col. 8 & 9 for the remainder of the important differences in anatomic pathology in the *upright* and *recumbent* positions. Similarly, obstructions of CSF flow were more pronounced in the *upright* position than in the *recumbent* position (Table 2A, col. 10 & 11).

Upright and Recumbent MR Images of Multiple Sclerosis Patients

Upright (and recumbent) MR images of the MS patients and normal examinees are presented in Figures 1–16.

The compared upright and recumbent MR imaging findings of the brain and cervical spine of the Multiple Sclerosis patients are described in Figures 1–8. The MR images of the normal examinees are contained in Figures 9–15.

As described in Figures 1–8, ***ALL*** MS patients exhibited specific anatomic pathologies of the cervical spine and corresponding obstructions of CSF flow. Four of the MS patients (MS patients #1, #2, #3 and #7) exhibited severe anatomic pathology, while the remaining four (MS patients #4, #5, #6 and #8) exhibited less striking cervical spine anatomic pathology that was nonetheless accompanied by significant obstructions to CSF flow (patient #4, Figures 4b, 4f, 4g: patient #5, Figures 5b, 5c, 5d: patient #6, Figures 6b, 6e) which CSF flow obstructions could result in increases in ventricular intracranial pressure (ICP), CSF leakages and the genesis of Multiple Sclerosis lesions. Additionally, the hydrocephalus of the occipital horns of the lateral ventricles (Figure 8e) and the ventricular dilatation of the body of the lateral ventricles (Figure 8b) are consistent with the likelihood of an increased ICP in patient #8.

The findings raise the possibility that interventions might be considered to restore normal intracranial CSF flow dynamics and intracranial pressure (ICP) as well as surgical procedures to correct the causative anatomy if non-invasive procedures prove insufficient.

Discussion

Struck and Haughton have pointed out in their study of CSF *flow* obstruction in Chiari patients that "the increased CSF flow *velocities* are associated with steeper pressure gradients across the foramen magnum" (10).

Alperin *et al*. have further established that there is a linear correlation between the measured CSF pressure gradient and the measured CSF Intracranial Pressure (ICP) when CSF dynamics are measured *in vivo* (11). As Alperin reported, "A twofold increase in the amplitude of the oscillating pressure (ICP) yielded a twofold increase in the amplitude of the pressure gradient" (11, p. 881).

Accordingly, the elevated peak CSF *velocities* measured in the MS patients of this study would indicate the existence of elevated intracranial pressures (ICP) in these MS patients.

Additionally, three of the eight MS patients (Table 2A, col. 6 & 7, patients #2, #4 and #5) *directly* exhibited elevated peak-to-peak CSF pressure gradients by MRI.

Accordingly, the increases in the peak-to-peak pressure gradients of these MS patients and the accompanying ICP increases can directly be the origin of the CSF "leaks" that appear evident in MS patient images and evident in their *peri-ventricular distribution* (Figure 1a, Figures I, II). Consistent with the findings of Struck and Haughton (10), the MS patients of this study who exhibited elevated CSF peak **inflow** *velocities* in the *upright* position (Table 2A, col. 4, patients #2 and #5, 1.047, .731) also exhibited elevated peak-to-peak pressure gradients when upright (Table 2A, col. 6, .054, .050 mmHg/cm) as compared to the normal examinees (Table 2B, col. 6, .0177).

The existence of peri-ventricular interstitial edema, Figure 1–8, in the MR images of the brain of all eight of the MS patients of this study is further consistent with the prospect that an increase in ICP is playing a role in generating MS "plaque" lesions.

The Possible Role of CSF "Leaks" in the Genesis of MS Lesions

The most important finding of this study is that cerebrospinal fluid "leaks" from the ventricles of the brain into surrounding brain parenchyma, possibly secondary to trauma induced blockages of CSF flow and resulting increases in ICP, may be playing an important *etiologic role* in the genesis of Multiple Sclerosis. The existence of such possible CSF "leaks" contributing to MS plaque formation could not be known until MS plaques themselves became readily visible on medical images. The advent of MRI made this a reality (1). Such CSF "leaks" could not have been seen prior to MRI, and a role for CSF "leakage" in the genesis of MS could not have been known prior to the advent of MRI and prior to the availability of phase coded MR imaging. These combined technologies have now made CSF flows directly visible and quantifiable.

The first suggestion of this possibility arose from the T_2 weighted sagittal brain image of a patient with MS (Figure 1a, patient #1) displaying an explicit CSF connection between ventricular CSF and one of the patient's MS lesions (Figure 1a, arrow #1). Another lesion in the same image exhibits a similar direct connection to ventricular CSF but in a less striking manner (Figure 1a, arrow #2). In addition, the *peri-ventricular distribution* of MS lesions naturally gives rise to the question that if MS lesions are not correlated in any way to CSF hydrodynamics, why are they not randomly distributed *throughout* the white matter of the brain, instead of being clustered around the ventricles of the brain. Further consistent with the possibility that MS plaques originate as CSF "leaks" secondary to trauma, is the existence of Dawson's fingers (Figure I) where the "long axis of the (MS) plaque" is "*parallel* with the *white matter fibers* in the corona radiata", i.e., not within the white matter fibers themselves but *parallel* to them. "Dawson's fingers" might well be the "leak" pathways of cerebrospinal fluid originating in the ventricle and joining the body of the MS plaque within the brain parenchyma. *Parallel* to the white matter fibers would be the path of least resistance for "leaking" CSF to diffuse within the brain parenchyma, i.e., *alongside* the white matter fibers.

Protein is the principal ingredient, other than water, of the cerebrospinal fluid. CSF contains approximately 15 to 40 mg/dL of protein (12). CSF gel electrophoresis has estab-

lished that there are "more than 300 polypeptides in CSF" (13). In addition, "nine antigenic species have been demonstrated in CSF that are absent in serum" (14). The question naturally arises whether the "leakage" of these CSF antigenic proteins, like the antigenic tau proteins they are known to contain (15), could be the source of the antigens generating the autoimmune reactions known to be the origin of MS lesions.

If trauma induced "leakage" of CSF proteins into the surrounding brain parenchyma, and particularly "leakage" of antigenic proteins, is contributing to the formation of MS plaques, then the vascular expansion stenting of the Azygous and Internal Jugular Veins recommended by Zamboni *et al*. (16) could be *monitored after installation* by UPRIGHT® phase coded MRI *measurements of CSF flow*. *Upright* phase coded imaging of CSF flow would assure that installed expansion stents are achieving the corrections of CSF flow dynamics and intracranial pressure (ICP) that are needed to terminate plaque generating CSF "leaks".

It is possible that those patients who currently do not respond to the Zamboni vein expansion stents or those who relapse are relapsing or not responding because the necessary restoration of normal CSF hydrodynamics and normal ICP has not been fully accomplished by the initial venous stenting procedure or is not being maintained.

Schoser *et al*. have reported that an increase in ICP is associated with an increase in blood velocity in the straight sinus (17). One possible explanation, therefore, for the success of the Zamboni *et al*. expansion stent procedure (16) could be that the Zamboni expansion stent is diminishing blood flow velocity in the straight sinus and BVR (Basil Vein of Rosenthal), thereby reducing ICP and diminishing plaque generating CSF "leaks".

Alperin *et al*. increased the measured ICP in their experimental animal (baboon) by restricting "jugular venous outflow" by "applying pressure over the neck region". The reduced "jugular venous outflow" resulted in an increase in the animal's measured intracranial pressure (ICP), demonstrating that reduced "jugular venous outflow can result in increased ICP". The reduced jugular venous outflow observed by Zamboni to exist in MS patients further suggests the presence of an elevated intracranial pressure in MS patients and that the successful response of MS patients to Zamboni *et al.*'s placement of expansion stents placed in the Internal Jugular Vein is the result of lowering MS patients' ICP closer to normal.

Noteworthy in this context is the recent report by McKee *et al*. who found abnormal forms of the immunoreactive tau proteins in lesions in the brain and spinal cords of professional athletes who had experienced repetitive head trauma (18). Since the tau proteins are a normal component of CSF (12), the possibility arises that "leaks" of ventricular CSF (Figures 1a, I, II, 1g, 1h, 2c, 3d, 4c, 4d, 5f, 5g, 7d, 7e, and 7f), secondary to trauma, could also be the origin of the antigenic tau proteins found in these repetitive head trauma patients (18).

In addition, the tau proteins have been identified as a significant participant in Alzheimer's disease. The possibility that they too are originating in the ventricular CSF, possibly secondary to increases in ICP, raises the prospect that Alzheimer's may also be the result of pathologic CSF hydrodynamics, which if corrected could halt the progress of Alzheimer's symptoms. Accordingly, while multiple authors (6,7,8) have fruitfully called attention to the correlation between trauma and the onset of MS, perhaps the "missing link" to date has been the inability to directly "see" the CSF "leaks" and CSF flow obstructions that have now been made visible by phase coded MR imaging. This new power

to dynamically visualize CSF hydrodynamics and its abnormalities opens the prospect of medically restoring pathologic CSF flow dynamics to normal under MR image guidance, thereby eliminating pathogenetic CSF leakages and the symptomatologies to which they give rise.

Myelogenesis is a normal physiologic process that repairs damaged myelin over time (19). If the myelin injuring process, i.e., "leaked" antigenic CSF proteins, could be terminated, there is the possibility that with the continuing injury from CSF "leakage" terminated, the demyelinated axons of MS lesions could be remyelinated by normal physiologic myelogensis and the MS lesions repaired.

The findings further suggest that going forward, victims of Motor Vehicle Whiplash injuries with persisting symptoms, e.g., headache, neck pain, should be scanned by UPRIGHT® MRI to assure that their CSF hydrodynamics and cervical anatomy (C1-C7) are normal. Should their CSF hydrodynamics prove abnormal, they should be monitored by UPRIGHT® MRI to assure they are restoring to normal over time, or ultimately decompressed by expansion stenting or cervical realignment if they are not.

Cervical Spine Trauma Pathology and Resulting CSF Flow Obstructions May Increase ICP and Produce Plaque Generating CSF "Leakage"

In conclusion, the results of our investigation suggest that Multiple Sclerosis may be biomechanical in origin wherein traumatic injuries to the cervical spine result in cervical pathologies that impede the normal circulation of CSF to and from the brain. The resulting obstruction of CSF **outflow** from the brain impairs the outflow of CSF from the lateral ventricles of the brain where 500 cc of cerebrospinal fluid is generated daily by the choroid plexuses (20). The obstruction to CSF **outflow** would result in an increase in ventricular CSF pressure (ICP) which in turn could result in "leakage" of cerebrospinal fluid and its content of more than 300 polypeptides and at least six (6) antigenic proteins (e.g., tau proteins) into surrounding brain parenchyma. The attachment of antigenic proteins to surrounding brain nerve fibers would stimulate the antigen-antibody reactions that produce the axon demyelinations characteristic of MS.

The authors wish to thank Scott Rosa, David Harshfield, Francis Smith and Jevan Damadian, *et al*. for initiating the use of the FONAR UPRIGHT® Multi-Position™ MRI technology for visualizing cerebellar tonsil ectopia (CTE) in automobile whiplash injuries (21). Their demonstration of the power of the FONAR UPRIGHT® Multi-Position™ MRI technology for imaging brain injury patients prompted us to enquire about the role of brain injury in Multiple Sclerosis when we observed, for the first time, the ventricular CSF connection to an MS lesion that was seen in patient #1.

References

1. Young, I.R., Hall, A.S., Pallis, C.A., Bydder, G.M., Legg, N. J., Steiner, R.E. (1981) *Lancet*, 318:1063–1066.
2. Lakhanpal, S.K. and Maravilla, K.B. (1999) in *Magnetic Resonance Imaging*, Eds. Stark, David D., Bradley, Jr., William G., Edition III, p. 1381, Figure 61-2, 61-3, Mosby, Inc.
3. Alperin, N., Sivaramakrishnan, A., Hushek, S.G., (2005) *Journal of Magnetic Resonance Imaging*, 22:591–596.

4. Haughton, V.M., Korosec, F.R., Medow, J.E., Dolar, M.T., and Iskandar, B.J. (2004) *AJNR, Am. J. Neuroradiol.*, 24:169.
5. Ouchi, Y., Nobezawa, S., Yoshikawa, E., Futatsubashi, M., Kanno, T., Okada, H., Torizuka, T., Nakayama, T. and Tanaka, K. (2001) *J. Cerebral Blood Flow and Metabolism*, 21, p. 1058 (1058–1066).
6. Brain, W., Wilkinson, M. (1957) *Brain* 80:456–478.
7. Poser, C.M. (2000) *Arch. Neurol.* 57:1074–1077.
8. Martinelli, V. (2000) *Neurol. Sci*., 21:5849–5852.
9. Bunketorp, L., Nordholm, L., Carlsson, J. (2002) *Eur. Spine J*. 11:227 (227–234).
10. Struck, A.F and Haughton, V.M. (2009) *Radiology* 253, No. 1, p. 185.
11. Alperin, N., Lee, S., Loth, F., Raskin, P., Lichtor, T. (2000) *Radiology* 217:877–885, Figure 8.
12. Felgenhauer, K. (1974) *Klin. Wochenschr*. 52(24):1158–1164.
13. Merril, C.R., Goldman, D., Sedman, S.A., Ebert, M.H. (1981) *Science* 211:1437–1438.
14. Laterre, C., Heremans, J., Carbonara, A. (1964) *Clin. Chim. Acta.* 10:197.
Bock E. (1973) *A Manual of Quantitative Immunoelectrophoresis*, Axelen, N.H., Kroll, J., Weeke, B., Eds., *Universitetsforlaget,* Oslo, pp. 119–124.
15. Sjögren, M., Vanderstichele, H., Ågren, H., Zachrisson, O., Edsbagge, M., Wikkelsø, C., Skoog, I., Wallin, A., Wahlund, L., Marcusson, J., Nägga, K., Andreasen, N., Davidsson, P., Vanmechelen, E., Blennow, K. (2001) *Clinical Chemistry* 47: 1776–1781.
16. Zamboni, P., Galeotti, R., Menegatti, E., Malagoni, A., Gianesini, S., Bartolomei, I., Mascoli, F., Salvi, F. (2009) *J. Vascular Surgery* 50(6):1348–1358.
17. Schoser, B., Reimenschneider, N., Hansen C. (1999) *J. Neurosurg*. 91:744–749.
18. McKee, A., Gavett, B., Stern, R., Nowinski, C., Cantu, R., Kowall, N., Perl, D., Hedley-Whyte, E., Price, B., Sullivan, C., Morin, P., Lee, H., Kubilus, C., Daneshvar, D., Wulff, M., Budson, A. (2010) *J. Neuropathol. Exp. Neurol*. 69(9):918–929.
19. Xin, M., Yue, T., Ma, Z., Wu, F., Gow, A. and Lu, Q. (2005) *J. Neurosci*. 25(6):1354–1365.
20. Department of Neurological Surgery, Columbia University Medical Center (http://www.columbianeurosurgery.org/conditions/adult-hydrocephalus).
21. Freeman, M., Rosa, S., Harshfield, D., Smith, F., Bennett, R., Centeno, C., Kornel, E., Nystrom, A., Heffez, D., Kohles, S. (2010) *Brain Injury*, 24(7–8):988–994.

Received June 8, 2011;
accepted June 22, 2011.